REPORT DOCUMENTATION PAGE

Form Approved
OMB No. 0704-0188

1. Agency Use Only (Leave Blank).	2. Report Date.	3. Report Type and Dates Covered.
	June 2001	Final Report

4. Title and Subtitle.

Use of Marine Mammal Vocalizations for Tracking 3-D and Geophysical Inversions

5. Funding Numbers.

N00014-97-1-0593

Project No.
Task No.

6. Author(s).

W. Kuperman

7. Performing Monitoring Agency Names(s) and Address(es).

University of California, San Diego
Marine Physical Laboratory
Scripps Institution of Oceanography
San Diego, California 92152

8. Performing Organization Report Number.

9. Sponsoring/Monitoring Agency Name(s) and Address(es).

Office of Naval Research
Ballston Centre Tower One
800 North Quincy Street
Arlington, VA 22217-5660
Robert Gisiner, ONR 335

10. Sponsoring/Monitoring Agency Report Number.

11. Supplementary Notes.

12a. Distribution/Availability Statement.

Approved for public release; distribution is unlimited.

12b. Distribution Code.

13. Abstract (Maximum 200 words).

Recordings of marine mammal vocalizations collected by large aperture hydrophone arrays in Summer, 1996, will be used to determine anatomical and behavioural information on the vocalizing animal. Recently developed advanced signal processing techniques in the fields of human speech processing and underwater acoustics will be modified and applied for this purpose. This information provides valuable input into studies of the effects of manmade sounds on marine mammals and on the use of underwater acoustic data in marine mammal census surveys.

14. Subject Terms.

marine mammal vocalizations, hydrophone arrays, signal processing techniques

15. Number of Pages.

2

16. Price Code.

17. Security Classification of Report.	18. Security Classification of This Page.	19. Security Classification of Abstract..	20. Limitation of Abstract.
Unclassified	Unclassified	Unclassified	None

Use of Marine Mammal Vocalizations for Tracking 3-D and Geophysical Inversions

Final Report

W. Kuperman

Supported by the
Chief of Naval Research
N00014-97-1-0593
June 1, 1997 - December 31, 2000

Abstract

Recordings of marine mammal vocalizations collected by large aperture hydrophone arrays in Summer, 1996, will be used to determine anatomical and behavioural information on the vocalizing animal. Recently developed advanced signal processing techniques in the fields of human speech processing and underwater acoustics will be modified and applied for this purpose. This information provides valuable input into studies of the effects of manmade sounds on marine mammals and on the use of underwater acoustic data in marine mammal census surveys.

Research Summary

The first two years of this grant, 1 June, 1997 through 31 May, 1999, covered graduate student expenses for Aaron Thode. Aaron finished his Ph.D. thesis in June, 1999, one year ahead of schedule.A listing of published works following this report document, among many things, the inversions for blue whale source time functions (i.e., the removal of propagation effects from recorded animal calls), and calling interactions between individuals.

The last year of this grant, 1 June, 1999 through 31 May, 2000, paid the graduate student expenses for K. Megan McArthur. The work for Megan's thesis, titled "Geoacoustic Inversions and Propagation Modeling in a Very Shallow Water Environment", is scheduled to be finished in the summer of 2001. Also, the abstracts for the presentation she gave on some of her research results to the Acoustical Society of America meeting are also listed. Also enclosed is a Marine Physical Lab technical memorandum that Megan published last year covering one aspect of her research

Publications

Thode, Aaron M., D'Spain, G. L., and W. A. Kuperman. "Matched-field Processing, Geoacoustic Inversion, and Source Signature Recovery of Blue Whale Vocalizations". J. Acoust. Soc. Am., 107(3), pp. 1286-1300. (2000).

Thode, Aaron M., Kuperman, W. A., D'Spain, G. L., and W. S. Hodgkiss, "Localization using Barlett Matched-Field Processor Sidelobes". J. Acoust. Soc. Am. 107(1), pp. 278-286 (1999).

McArthur, K. M. and W. S. Hodgkiss. "Geoacoustic Inversion in a Very Shallow Water Environment". J. Acoust. Soc. Am., 106(4), p. 2133 (1999).

D'Spain, G. L., McArthur, K. Megan, Deane, Grant B., and W. Kendall Melville. "Use of Surfseisms for Determining Near-Surf-Zone Properties". J. Acoust. Soc. Am., 106(4), p. 2133 (1999).

Thode, A.M., G.L. D'Spain, and W.A. Kuperman, "Physical constraints on blue whale sound production mechanisms derived from matched-field processing", J. Acoust. Soc. Am. (submitted, 1999).

McArthur, K. Megan. "Sediment Survey of the Nearshore Region at Las Pulgas Beach, Camp Pendleton, California". MPL Technical Memorandum 464, Marine Physical Laboratory, Scripps Institution of Oceanography, San Diego, 37 pgs. (1999).

Thode, Aaron. "Localization, Inversion, and Source Signal Recovery of Blue Whale Sounds using Matched Field Processing". Ph.D. Dissereation, Scripps Institution of Oceanography (1999).

ONR/MPL REPORT DISTRIBUTION

Office of Naval Research (3)
Department of the Navy
Ballston Tower One
800 North Quincy Street
Arlington, VA 22217-5660
Atten: Robert Gisiner, ONR 335

Regional Director (1)
ONR Detachment
San Diego Regional Office
4520 Executive Drive, Suite 300
San Diego, CA 92121-3019

Commanding Officer (1)
Naval Research Laboratory
4555 Overlook Avenue, S.W.
Attn: Code 2627
Washington, D.C. 20375-5320

Defense Technical Information Center (4)
8725 John J. Kingman Road
Suite 0944
Ft. Belvoir, VA 22060-6218

ONR/MPL REPORT DISTRIBUTION

Office of Naval Research (3)
Department of the Navy
Ballston Tower One
800 North Quincy Street
Arlington, VA 22217-5660
Atten: Robert Gisiner, ONR 335

Regional Director (1)
ONR Detachment
San Diego Regional Office
4520 Executive Drive, Suite 300
San Diego, CA 92121-3019

Commanding Officer (1)
Naval Research Laboratory
4555 Overlook Avenue, S.W.
Attn: Code 2627
Washington, D.C. 20375-5320

Defense Technical Information Center (4)
8725 John J. Kingman Road
Suite 0944
Ft. Belvoir, VA 22060-6218

Localization using Bartlett matched-field processor sidelobes

Aaron M. Thode, W. A. Kuperman, G. L. D'Spain, and W. S. Hodgkiss
Marine Physical Laboratory, Scripps Institution of Oceanography, San Diego, California 92093-0205

(Received 8 May 1998; revised 28 April 1999; accepted 20 September 1999)

Ambiguity surface sidelobes generated by the Bartlett matched-field processor (MFP) shift location with frequency. This sidelobe shift can be viewed as a continuous trajectory in a range-frequency plane at a fixed depth, where the trajectories converge to the correct source range for a perfectly matched surface. In isovelocity or bottom-interacting environments the sidelobe trajectories are straight lines that converge to the true range at zero frequency, while environments with upward-refracting sound-speed profiles have trajectories that asymptotically converge as the frequency approaches infinity. This behavior can be explained by the theory of waveguide invariants, which predict the local behavior of interference maxima/minima of acoustic intensity in the frequency-range plane. As the ambiguity surface of the Bartlett matched-field processor has a physical interpretation in terms of a time-reversed acoustic field, with the sidelobes analogous to local interference maxima, these invariant concepts can be reformulated for application to MFP. These interference trajectories are demonstrated to exist in simulations, broadband source tows, and a type A blue whale vocalization. Sidelobe trajectories also exist in the range-depth plane, but they contain no information about the correct source depth. An appendix demonstrates how these sidelobe properties can be exploited when combining ambiguity surfaces through use of gradient and Radon transform information. The resulting range estimators demonstrate better peak-to-sidelobe ratios than a simple incoherent average.
[S0001-4966(00)01001-8]

PACS numbers: 43.30.Pc, 43.30.Sf [DLB]

INTRODUCTION

This paper shows that sidelobes of the Bartlett matched-field processor (MFP) contain information about both the source location and the waveguide environment. The derivation of these properties is a straightforward extension of the acoustic invariant concept as first developed by Chuprov[1] and extended in subsequent papers.[2,3] These sidelobe properties are demonstrated to exist in both simulations and data.

Bartlett ambiguity surfaces typically are incoherently averaged across frequency when performing matched-field processing on a broadband source.[4] This method assumes that the true source location at each frequency remains fixed, while the sidelobes will appear at different locations at different frequencies, and thus will be suppressed by the averaging. This shift of sidelobe location with frequency can be viewed as a continuous trajectory in a range-frequency plane, where the depth is fixed and the Bartlett surfaces are generated at small increments of frequency. These trajectories form patterns that converge to the true source range and their shape is dependent on the type of waveguide being modeled.

Section I presents the derivation of these trajectories in the range-frequency plane for perfectly matched, range-independent environments. Section II provides examples of these patterns in simulation and data. In Appendix A we address the behavior of sidelobe trajectories with ambiguity surface depth. Finally, in Appendix B we discuss two simple postprocessing methods for improving the peak-to-sidelobe performance of frequency-averaged Bartlett surfaces, using these sidelobe properties. This appendix will also demonstrate that the correct range of a source can be recovered from sidelobe information alone.

I. DERIVATION OF SIDELOBE TRAJECTORIES IN THE RANGE-FREQUENCY PLANE

In this section the Bartlett surfaces will be assumed to be generated from range-independent, perfectly matched environments. The case of mismatched MFP surfaces is the subject of later work.

At ranges greater than a few water depths, a source at depth z_s and range R will produce a pressure field at a depth z_n that can be expressed as a sum of normal modes.[5]

$$p(z_n,z_s,R,\omega)=p(z_n)$$
$$=\frac{ie^{-i\pi/4}}{\rho(z_s)\sqrt{8\pi R}}\sum_l U_l(\omega,z_s)U_l(\omega,z_n)\frac{e^{i\xi_l(\omega)R}}{\sqrt{\xi(\omega)_l}}, \quad (1)$$

where ξ is the horizontal wave number of the lth mode, and n is the index of the receiving hydrophone along a vertical array. Similarly, a normalized MFP replica generated by a hypothetical source at range, depth (r,z) will have the form

$$\hat{p}(z_n,z,r,\omega)=\hat{p}(z_n)$$
$$=N\sum_l \hat{U}_l(\omega,z)\hat{U}_l(\omega,z_n)\frac{e^{i\hat{\xi}_l(\omega)r}}{\sqrt{\hat{\xi}_l(\omega)r}}, \quad (2)$$

where N is a normalization constant. The complex pressure field received across a vertical array of hydrophones can be expressed as a vector, each element representing the field detected by a single receiving hydrophone. The Bartlett surface can be expressed as the power of the inner product between the vectors formed from (1) and (2):[4]

 1063-7834/2000/107(1)/9/$17.00

$$B(r,\omega,z)=\frac{|\Sigma_n p(z_n)\hat{p}^*(z_n)|^2}{\Sigma_n|p(z_n)|^2\Sigma_n|\hat{p}(z_n)|^2}. \tag{3}$$

For the case of a perfectly matched Bartlett processor, the expression can be simplified by assuming that the aperture of the array is sufficient to exploit the orthogonality of the modes:

$$\sum_n (\Delta z)U_l(\omega,z_n)\hat{U}_m(\omega,z_n)/\rho(z_n)=\delta_{lm}. \tag{4}$$

This approximation yields the following formula for the Bartlett ambiguity surface:

$$B(z_s,z,r,R,\omega)=N\sum_{l,m} P_l P_m \cos(\hat{\chi}_{lm}r-\chi_{lm}R),$$

$$\hat{\chi}_{lm}=\hat{\xi}_l-\hat{\xi}_m, \quad \chi_{lm}=\xi_l-\xi_m, \tag{5}$$

$$P_i=U_i(\omega,z_s)U_i(\omega,z)/\sqrt{\xi_i}.$$

The hatted variables represent the modeled environment, and the $r^{(-1/2)}$ terms have been merged with the normalization constant. Written this way, it is obvious that with the depth z fixed, the Bartlett function will show a series of interference maxima and minima, with the maxima corresponding to sidelobe locations. In order to locate the contours of constant correlation in the range-frequency plane, the total differential of the Bartlett surface is taken, following Brekhovskikh:[3]

$$dB=\frac{\partial B}{\partial r}dr+\frac{\partial B}{\partial \omega}d\omega=0, \tag{6}$$

where ω is the frequency of the source. Thus an expression for the slope of the contour is obtained:

$$\frac{\partial \omega}{\partial r}=-\frac{\partial B/\partial r}{\partial B/\partial \omega},$$

$$\frac{\partial B}{\partial r}\cong\sum_{l,m} P_l P_m \hat{\chi}_{lm}\sin(\hat{\chi}_{lm}r-\chi_{lm}R), \tag{7}$$

$$\frac{\partial B}{\partial \omega}\cong\sum_{l,m} P_l P_m\left[r\frac{\partial\hat{\chi}_{lm}}{\partial\omega}-R\frac{\partial\chi_{lm}}{\partial\omega}\right]\sin(\hat{\chi}_{lm}r-\chi_{lm}R).$$

To first order the mode shapes have been assumed independent of frequency, and the cylindrical spreading terms have been neglected. The expressions χ and $\delta\chi/\delta\omega$ can be redefined in terms of modal phase and group velocities c_p and c_g:

$$\chi_{lm}=\omega\left[\frac{1}{c_p^l}-\frac{1}{c_p^m}\right]\equiv\omega\Delta(1/c_p), \tag{8a}$$

$$\frac{\partial\chi_{lm}}{\partial\omega}=\left[\frac{1}{c_g^l}-\frac{1}{c_g^m}\right]\equiv\Delta(1/c_g). \tag{8b}$$

Following Brekhovskikh,[3] the phase slowness can be expressed as a Taylor expansion of the group slowness:[1]

$$\frac{1}{c_p^l}=\frac{1}{c_p^m}+\left(\frac{\Delta(1/c_p)}{\Delta(1/c_g)}\right)_{\omega,l,m}\left[\frac{1}{c_g^l}-\frac{1}{c_g^m}\right]. \tag{9}$$

Now assume that the number of modes in the system is large enough that mode order can be considered a continuous variable. Then, in the continuous limit, one can define the following quantity:

$$\beta\equiv-\frac{d(1/c_p)}{d(1/c_g)}. \tag{10}$$

This term, labeled the acoustic invariant by Chuprov,[1] is argued to be independent of mode order and frequency, provided that the frequency band in question is far from most modal cutoff frequencies. Equivalently stated, β is constant if the group velocities of a waveguide environment can be expressed as an explicit function of modal phase velocity only. Two standard examples of β that can be derived analytically are an isovelocity waveguide, and a so-called n^2 profile. These two cases will appear in the specific examples in Sec. II.

For an isovelocity waveguide with a perfectly reflecting bottom, the following relation holds:

$$c_p c_g=c^2, \tag{11}$$

where c is the speed of sound of the medium. Thus the phase velocity does not explicitly depend on mode order or frequency. Using Eqs. (10) and (11), β is

$$\beta=\cos^2\theta\approx 1, \tag{12}$$

where θ, the effective ray angle of the mode with respect to the horizontal, is small. This relationship applies to many shallow-water environments, even if the sound-speed profile is not strictly isovelocity.

Another example is a waveguide with a linear variation in the square index of refraction, i.e.,

$$n^2(z)=c_0^2/c_1^2=1-az, \tag{13}$$

where c_0 represents the surface sound speed. Note that a linear sound-speed profile is a special case of this form wherein $az\ll 1$. The group and phase velocities[1] are related by

$$c_g=\frac{3c_p}{2+(c_p/c_0)^2}. \tag{14}$$

The β for this environment can be written as

$$\beta=\frac{-3}{2-(c_p/c_0)^2}\approx -3, \tag{15}$$

where c_p has been assumed approximately equivalent to c_0.

These expressions for β are only approximate. In reality, different combinations of modes at different frequencies will show slightly different values of β. Also, a single environment can contain mode groups that have properties of both Eqs. (12) and (15). For example, a shallow-water environment with an upward-refracting profile may have low-frequency mode groups that obey Eq. (12), but once the frequency becomes large enough that a group of modes becomes trapped in the waveguide, Eq. (15) will become relevant. However, for the rest of this paper, β will be assumed constant for a particular environment.

Combining Eqs. (7)–(10) allows several terms that are independent of mode number to be factored outside the summations. Terms with an explicit dependence on mode num-

ber then cancel and an expression for the slope of a constant-correlation contour in the Bartlett range-frequency plane can be derived:

$$\frac{\partial \omega}{\partial r} = \beta \frac{\omega}{r - R}. \tag{16}$$

This differential equation can be solved for the curves of constant Bartlett intensity:

$$\omega = C(r - R)^{\beta}, \tag{17}$$

where C is a constant of the integration, independent of r. Because $\beta \approx 1$ is a good approximation for shallow-water waveguides, the trajectories in these environments are straight lines that converge to $r = R$, which is the true range.

To determine the value of the constant in (17) for shallow-water environments, the following approximation can be made for low-order modes in an ideal waveguide:[2]

$$\chi_{lm} \cong \frac{(l^2 - m^2) c \pi^2}{\omega D^2}, \tag{18}$$

where D is the depth of the waveguide. Since the distance between interference maxima generated between modes l and m is $2\pi/\chi_{lm}$, interference maxima will occur at ranges r where the following relationship holds:

$$r - R = \frac{2\pi k}{\chi_{lm}}, \quad k = 0, \pm 1, \pm 2, \ldots. \tag{19a}$$

The resulting expression for the Bartlett sidelobe trajectories in an ideal waveguide becomes

$$\omega = \frac{(l^2 - m^2) c \pi}{2kD^2}(r - R),$$

$$l, m = 1, 2, 3 \ldots, \quad k = 0, \pm 1, \pm 2, \ldots. \tag{19b}$$

The behavior of sidelobes with respect to ambiguity surface depth is discussed in Appendix A.

II. EXAMPLES

This section provides four examples of MFP sidelobe trajectories. Subsection A describes a simulation of an acoustic source in a shallow water environment. Subsection B uses data recorded in a similar environment from a broadband source tow off San Diego in 1994. Subsection C contains a simulation of a source in 2-km-deep water with a idealized Arctic profile (linear sound-speed profile). Lastly, subsection D demonstrates the patterns generated by a blue whale call recorded off the Southern California Channel Islands in 1996.

A. Shallow-water environmental simulation

This example uses an optimized geoacoustic model of the shallow water environment off Point Loma, San Diego, and is shown in Fig. 1. The model was constructed in conjunction with the SWellEx series of experiments performed in the area,[6,7] and consists of a basement of mudstone topped by a 26-m layer of slit. Using the normal-mode model Kraken,[8] a broadband acoustic source was modeled at 30-m depth and a range of 6 km from a 64-element vertical array placed in the lower half of the water column. No noise was added to the model. A series of Bartlett MFP ambiguity surfaces was generated using the same environment from 10 to 100 Hz. The results are stacked and viewed along the fixed depth of 30-m, and the resulting plot is shown in Fig. 2. The sidelobe trajectories clearly indicate the correct source range. The fact that the trajectories are straight indicates that a nearly isovelocity model has been used to generate the replica vectors.

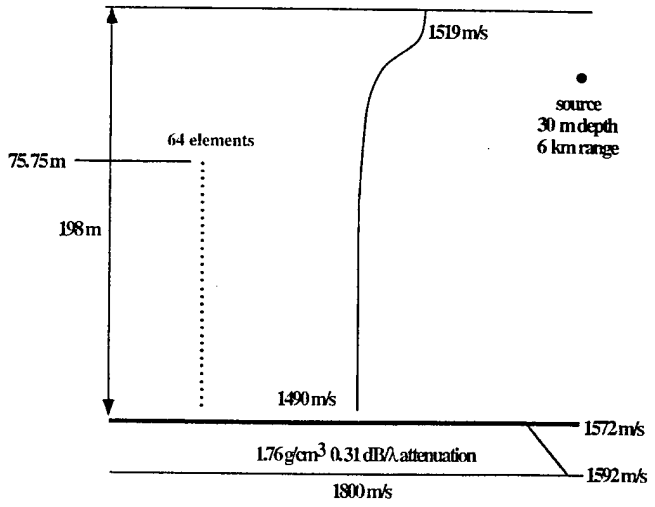

FIG. 1. Schematic of the shallow-water waveguide environment used in the simulations. The environment represents summer conditions off Point Loma, San Diego, CA. An acoustic source is simulated at 30-m depth and 6-km range, and its signal is received across a 120-m aperture vertical array with 64 elements spaced 1.875 m apart. The top element is at 75.75-m depth. The bottom is a 26-m layer of silt overlying a half-space of mudstone.

Figure 3 demonstrates that these interference patterns converge to the correct range when viewed along a fixed depth different from the true source depth. In this figure, the range-frequency plane was made along a fixed depth of 158 m, or 128 m deeper than the correct source depth.

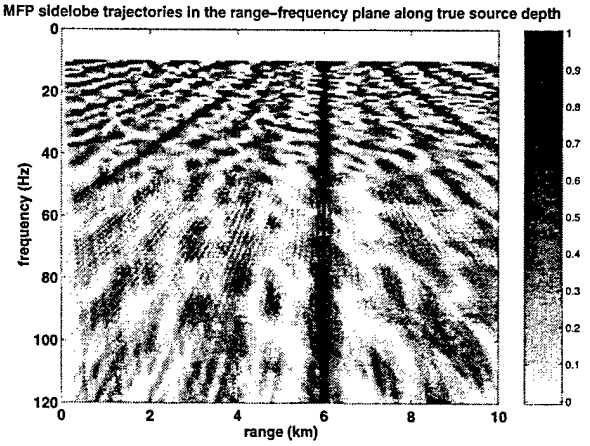

FIG. 2. The MFP sidelobe trajectories generated using the environment in Fig. 1, where $\beta \sim 1$. The intensity scale is a linear measure of the normalized Bartlett power. The replicas were generated using Kraken, using all 64 array elements. Low-order mode interferences are visible across the entire frequency band; higher-order mode interferences generate partial trajectories, because the sidelobes change depth with frequency. The vertical line indicates the presence of the mainlobe. All trajectories converge to the correct source range.

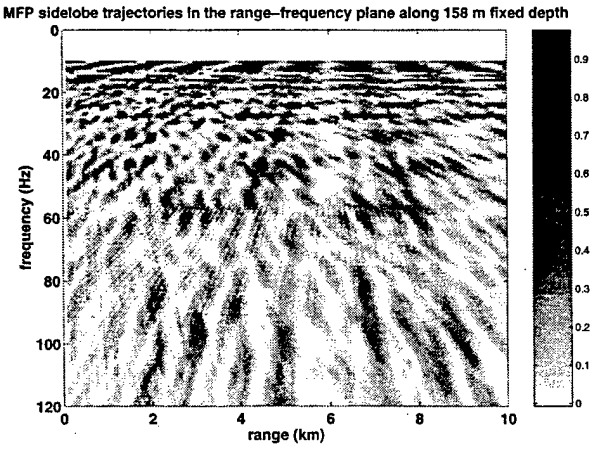

FIG. 3. Same as Fig. 2 but the range-frequency plane is viewed along an ambiguity surface depth of 158 m or 128 m deeper than the true source. While the mainlobe is absent, the sidelobe trajectories still converge to the true source range.

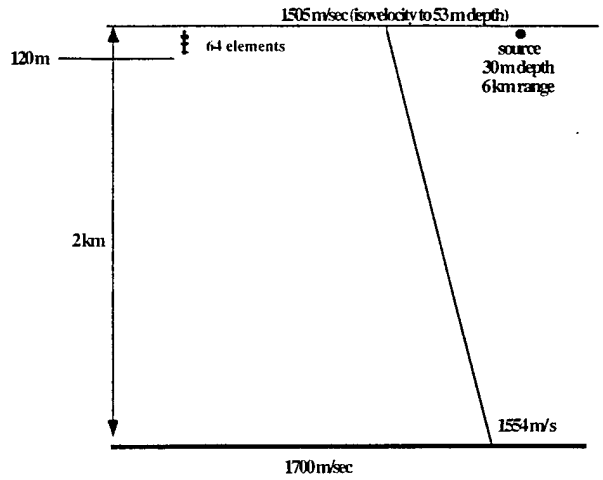

FIG. 5. Schematic of upward-refracting environment used for $\beta=-3$ simulation. The sound-speed profile is isovelocity at 1505 m/s to 53 m, then increases linearly to 1554 m/s at 2-km depth. The simulated source and receivers are at the same location as in Fig. 1. Note that the vertical array covers less than 10% of the water depth. The bottom consists of a 1700-m/s half-space.

B. Data from shallow-water environment

This example uses data from a source tow performed during the SWellEx-3 experiment conducted off the coast of San Diego[6] beginning on 27 July 1994 at 18:00 GMT. The J13 source projected pseudo-random noise at a 30-m depth over a 85–150-Hz bandwidth with a frequency-integrated source level of 170 dB *re* 1 μPa @ 1 m. The source was fixed in place during this time, and the bathymetry profile between the source ship and the vertical array was mostly range independent. The environmental model of Fig. 1 was used to produce the replicas for the MFP and a slice of the range-frequency plane at the correct source depth is shown in Fig. 4. As theory predicts, the sidelobes converge to the correct range of 6 km.

C. Arctic profile simulation

This example was constructed to demonstrate sidelobe trajectories in an environment where $\beta=-3$. Figure 5 outlines the model, which consists of a 2-km-deep ocean with an upward-refracting sound-speed profile and a bottom half-space of 1700 m/s. A 120-m aperture vertical array covering less than 10% of the water column is placed in the water, recording a signal produced by a source at 30-m depth and 6-km range. The poor coverage of the water column violates the orthogonality condition in Eq. (4), yet the result presented in Fig. 6 demonstrates that at low frequencies the sidelobe trajectories behave as predicted by Eq. (17). At higher frequencies the orthogonality condition fails and the trajectories blur and merge. For environments where β is negative, the trajectories asymptotically converge to the correct range at infinite frequency. This is a consequence of the fact that modal group velocity increases with phase velocity for this environment [Eq. (14)]. It is intriguing that a successful localization can be achieved with little vertical water column coverage.

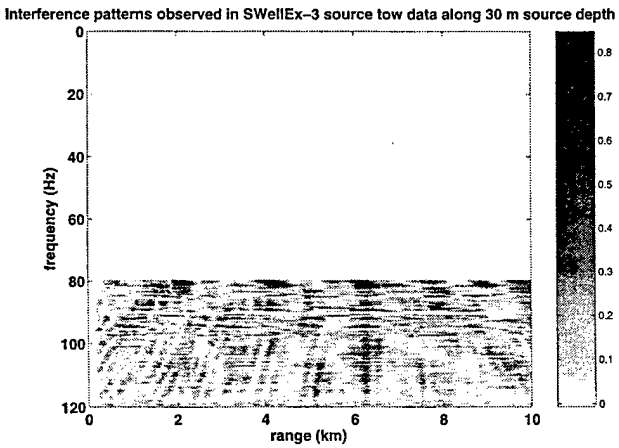

FIG. 4. Sidelobe trajectories generated from ocean acoustic data along a fixed depth of 30 m. The replicas from Fig. 1 were correlated with spectral estimates derived from 2.73 s of data recorded during the SWellEx-3 experiment. The true source location is 30-m depth and 6-km range. The signal consisted of pseudo-random noise with a bandwidth of 85–120 Hz.

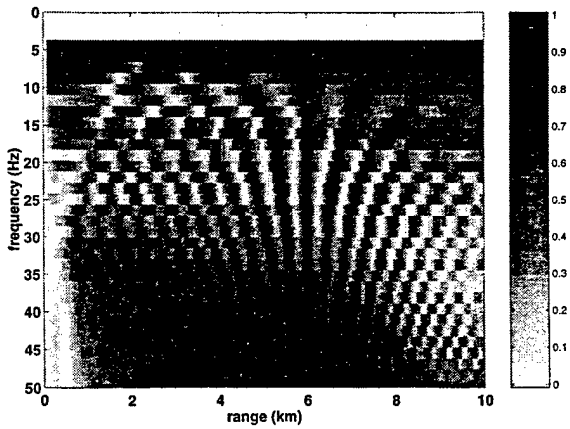

FIG. 6. The MFP sidelobe trajectories for the environment outlined in Fig. 5. The ambiguity function is sliced along the modeled source depth. In this type of environment the sidelobe trajectories converge asymptotically to the correct range as $f\to\infty$. The blurring of the individual trajectories above 40 Hz is likely due to insufficient water column coverage by the vertical array.

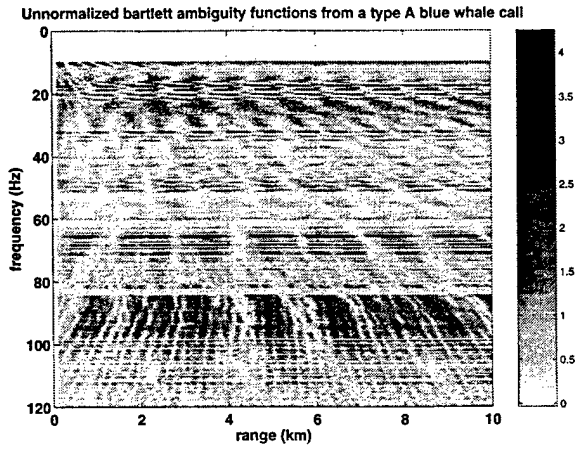

FIG. 7. Unnormalized backpropagated PE ambiguity range-frequency surface from a type A blue whale vocalization, recorded on Julian Day 203 at 20:52 GMT. Ten seconds of data have been used to form an averaged cross-spectral density matrix from which the eigenvector with the greatest eigenvalue was selected for backpropagation. The call contains energy bands at 17, 32, 48, 65, 95, and 110 Hz. The water depth was 128 m and the bottom speed was estimated to be ~1650 m/s.

D. Blue whale vocalization

This final example was obtained from processing a blue whale sound recorded off San Miguel Island in Southern California in 1996.[9] This vocalization is the "type A" call typically made by Northeastern Pacific populations[10] and generally lasts 15–20 s. It is a pulsed call with pulse period 0.7 s, containing energy in the 15–120-Hz frequency range. Resonances near 17, 34, 51, 65, 95, and 110 Hz result in a considerable variation in signal-to-noise ratio (SNR) with frequency. Typically the strongest frequency bands are between 17–20 Hz and 85–95 Hz.

The geoacoustic environment and sound-speed profile in this area were estimated using standard geoacoustic inversion methods,[11–13] on several high SNR calls. A very fast back-propagated PE algorithm[14] then was used to perform localization on other type A calls, including the one shown here. Holding the source depth constant at 15 m (a typical calling depth for the animal), the resulting range-frequency MFP plane for this call is shown in Fig. 7.

Two features from this figure merit further discussion. The first is the well-defined sidelobe patterns that lie between 85 and 120 Hz and which seem to converge to ~5-km range. The signal quality is worse at lower frequencies, but the convergence pattern is still visible in the frequency band between 65 and 75 Hz. Below 60 Hz a second feature appears: interference maxima and minima that converge to the range-frequency origin. This type of convergence often appears when processing signals with significant noise, or surfaces with severe environmental mismatch, particularly mismatch in vertical array tilt. A full explanation of this feature is involved and will be the subject of future work.

Ever when the relatively high SNR region between 85–120 Hz is incoherently averaged, the output reveals only a weak mainlobe with numerous high-amplitude sidelobes. In Appendix B we demonstrate how the sidelobe interference structure apparent in Fig. 7 can be exploited to improve the performance of the final averaged range estimate.

III. CONCLUSION

Broadband Bartlett matched-field processing sidelobes contain source location and environmental information, which is readily apparent when viewed in the range-frequency plane along a fixed ambiguity surface depth. The existence and shapes of the sidelobe trajectories can be derived using waveguide invariant theory. Several examples of these patterns using both simulation and ocean acoustic data have been presented. One intuitive explanation for this sidelobe behavior is that the Bartlett ambiguity surface has a physical interpretation in terms of a time-reversed acoustic field.[15] From this viewpoint, MFP sidelobes are analogous to zones of constructive interference in the ocean and should therefore contain useful information about the source location.

Two interesting research avenues follow from this fundamental observation. The first is that this sidelobe behavior can be exploited to improve the mainlobe-to-sidelobe performance of a broadband Bartlett processor. The exact details of how this can be achieved are complex and thus have been relegated to Appendix B. The second avenue concerns the effect of environmental mismatch and ocean noise on the structure of these patterns. As hinted in Sec. II D, the results are intriguing and are intimately intertwined with the concept of MFP "mirages."[16] A description of these properties will have to described separately.

ACKNOWLEDGMENTS

The authors would like to thank MPL technical staff and the crew of the R/P FLIP for making the collection of the data used in this paper possible. The contributions of Hee Chun Song and James Murray are particularly appreciated. This research was funded by the Office of Naval Research Grant No. N00014-97-0593 and N00014-96-0603.

APPENDIX A: DEPTH DEPENDENCIES OF SIDELOBE SHIFTS

In addition to the range shift discussed earlier. MFP sidelobes display spatial shifts along the depth axis with changes in frequency. According to the Wantzel–Kramers–Brillouin (WKB) approximation, a mode can be represented as a sum of $\exp(\pm i\gamma Z)$ terms where γ is the depth-dependent modal vertical wave number associated with a depth-dependent ray arrival angle $\theta = a\tan(\gamma/\xi)$. If the acoustic energy intercepting a vertical array is associated with a particular arrival angle, one of the exponential terms dominates and the Bartlett surface can be written as

$$B(r,z) \approx \sum_{l,m} \cos[\alpha_{lm}(z-z_s) + \chi_{lm}(r-R)],$$

$$\alpha_{lm} \equiv \gamma_l \gamma_m, \tag{A1}$$

from which can be derived

$$\frac{\partial \omega}{\partial z} = -\frac{\partial B/\partial z}{\partial B/\partial \omega}, \quad \frac{\partial B}{\partial z} = \sum_{l,m} \alpha_{lm} P_l P_m \sin(\chi_{lm}[r-R]),$$
$$\frac{\partial B}{\partial \omega} = \sum_{l,m} \frac{\partial \chi_{lm}}{\partial \omega}(r-R) P_l P_m \sin(\chi_{lm}[r-R]). \tag{A2}$$

Note that $\delta\gamma d\omega = 0$ reflecting the fact that mode shape is independent of frequency at this order (e.g., $\gamma_m = m\pi/D$ in an ideal waveguide). In order to factor the double sums, a relation is needed between α and $\delta\gamma/\delta\omega$. A Taylor series expansion can be constructed between the wave numbers:[1]

$$\gamma_l = \gamma_m + (\xi_l - \xi_m)\frac{d\gamma}{d\xi}. \tag{A3}$$

Simplifying

$$\frac{\alpha_{lm}}{\chi_{lm}} = \frac{d\gamma}{d\xi} = \frac{d\sqrt{k^2-\xi^2}}{d\xi} = -\frac{\xi}{\gamma} = -\cot\theta, \tag{A4}$$

one obtains, using (8),

$$\alpha_{lm} = \frac{d\gamma}{d\xi} = \beta\omega\cot\theta\frac{\partial\chi_{lm}}{\partial\omega}, \tag{A5}$$

which, when combined with (A2), yields

$$\frac{\partial\omega}{\partial z} = -\beta\frac{\omega}{r-R}\cot\theta. \tag{A6}$$

One sees that sidelobes trajectories generated by high-order modes experience greater shifts in the vertical than those from low-order modes. These shifts are not large. The low-order sidelobes generated by a 50 Hz source in a 200-m-deep ideal waveguide will shift around 3-m depth per kilometer range. Note also that the true source depth does not appear anywhere in Eq. (A6), a consequence of the fact that $\delta\gamma/\delta\omega \approx 0$. Therefore, the sidelobe trajectories in the z-ω plane should contain no source depth information.

The trajectories generated by the lower-order modes shift vertically only a small amount with a change in frequency. Thus, in Fig. 2 the low-order trajectories remain visible over a large frequency range at 30-m depth. By contrast, the finer-scale intensity trajectories shift considerably in the z direction across this frequency range so only partial trajectories for the high-order modes are visible.

APPENDIX B: TWO ALGORITHMS FOR IMPROVING RANGE ESTIMATION USING SIDELOBES

One potential application investigated here is the possibility of "enhancing" incoherent broadband Bartlett averaging by exploiting knowledge of sidelobe behavior. The first method uses a simple trick to effectively cancel all sidelobes during averaging, and the second method uses the Radon transform to estimate the range at which all sidelobe trajectories converge. Using this latter approach it is possible to obtain a correct range estimate without using the mainlobe, which suggests that the mainlobe does not even have to lie on the plot.

To illustrate both methods, a simple, abstracted model of a MFP range-frequency plane is shown in Fig. B1(a). The model represents a shallow-water environment wherein the

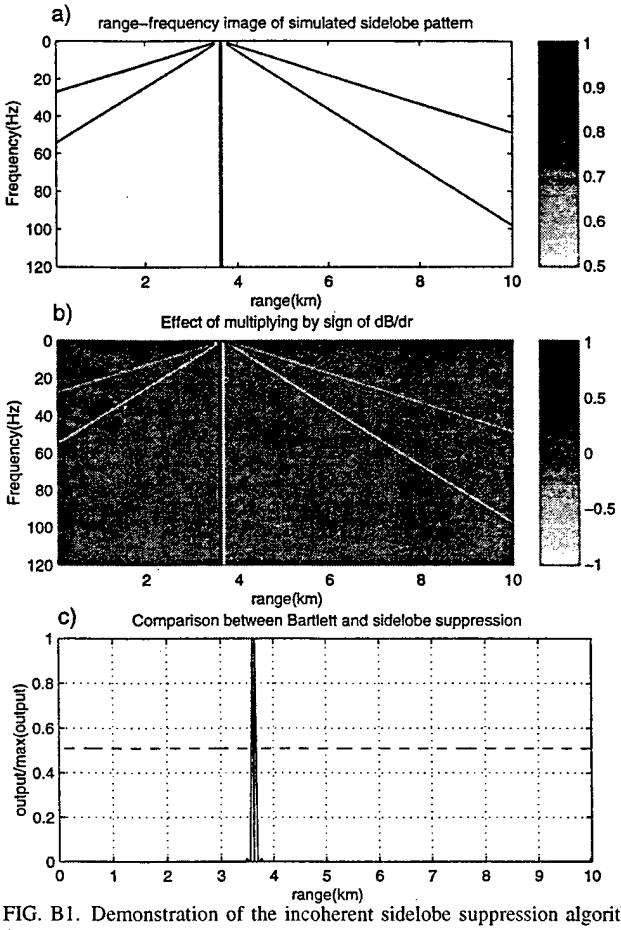

FIG. B1. Demonstration of the incoherent sidelobe suppression algorithm. (a) Simple abstracted model of sidelobe trajectories in a MFP range-frequency plane. Each trajectory is three range bins wide and is assigned a value of one. Other range-frequency bins are assigned a value of 0.5. (b) Effect of multiplying a by $(\partial B(r,\omega)/\partial r)B(r,\omega)$. (c) Result of averaging along the frequency axis in (b).

mainlobe lies at 3.75 km and four sidelobes converge to the correct range at 0 Hz from angles of ± 45 and ± 62 degrees from the vertical. At every frequency the sidelobes and mainlobe are three range bins wide and each of these bins is assigned a value of one. During standard broadband MFP processing, the ambiguity surfaces are averaged [i.e., an integration is performed along a vertical line for each range bin in Fig. B1(a)]

$$\bar{B}_0(r) = \frac{\Delta\omega}{\omega 2 - \omega 1}\int_{\omega 1}^{\omega 2} B(r,\omega)\, d\omega, \tag{B1}$$

where B represents the Bartlett ambiguity function and $\Delta\omega$ is the width of a frequency bin in rad/s. Examination of this example suggests that if positive values could be assigned to the left edge of each trajectory and negative values to the right edge, then the sidelobe at frequency $\omega + \delta\omega$ will tend to cancel out the sidelobe at frequency ω. An easy way to achieve this is to multiply each ambiguity surface by the sign of its derivative with respect to r:

$$\bar{B}_1(r) = \frac{\Delta\omega}{\omega 2 - \omega 1}\left\| \int_{\omega 1}^{\omega 2} \operatorname{sgn}\left(\frac{\partial B(r,\omega)}{\partial r}\right) B(r,\omega)\, d\omega \right\|. \tag{B2}$$

The effect of performing this operation on our sample surface is shown in Fig. B1(b). As desired, every trajectory now

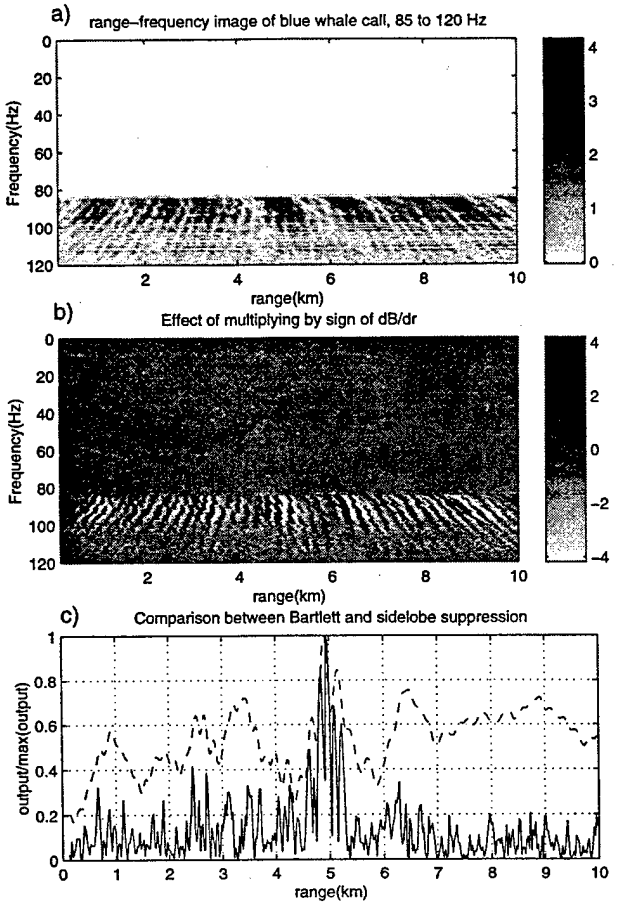

FIG. B2. Demonstration of the incoherent sidelobe suppression algorithm on the data shown in Fig. 7. (a) Reproduction of Fig. 7, retaining only the frequencies above 85 Hz. (b) Effect of multiplying by $(\partial B(r,\omega)/\partial r)B(r,\omega)$. (c) Comparison of Eq. (B2) (solid line) with the standard Bartlett average given in B1 (dashed line). Both curves are normalized relative to their maximum values.

has a value of $+1$ on the left edge and -1 on the right. When integrated vertically, every positive value on the sidelobe is canceled by a negative at an adjacent frequency, except for the vertical trajectory (mainlobe). In that case, all the positive and negative values add constructively and the sharp spike displayed in Fig. B1(c) is obtained.

Figure B2 illustrates the effectiveness of this simple postprocessing on the blue whale ambiguity function shown in Fig. 7. Figure B2(a) shows the 85–120-Hz: band region of this function. Applying Eq. (B2) produces the surface in Fig. B2(b), and averaging across frequency then yields the solid-line output in Fig. B2(b). For comparison the regular Bartlett average from Eq. (B1) is plotted as a dashed line. Both plots are normalized with respect to their maximum values. It is clear that Eq. (B2) generates a result with lower peak-to-sidelobe ratios (2.5) than regular averaging (1.25), while requiring little additional computational effort.

A more exotic approach than sidelobe suppression involves estimating the range at which the sidelobe trajectories converge—a "sidelobe beamformer." If a shallow water environment is being modeled so that $\beta \approx 1$, then the sidelobe trajectories are straight lines. Thus, the integral from Eq. (B2) can be modified to allow the integration path to transect

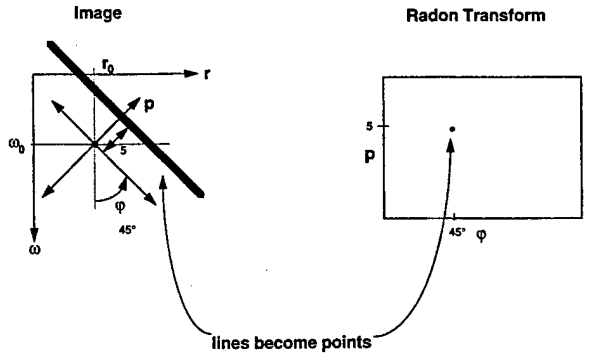

FIG. B3. Illustration of the Radon transform. Given a reference point (r_0,ω_0), the transform outputs line integrals as a function of rotation angle φ from the vertical and unitless distance p along the p axis. Thus straight lines in the image are transformed into points in the (p,φ) plane.

the image along any angle φ with respect to the frequency (vertical) axis beginning from the point $(r,0)$:

$$\bar{B}_2(r,\varphi) \equiv \frac{1}{N(r,\varphi)} \left\| \int_0^T B_e(r(t),\omega(t))\,dt \right\|,$$

$$B_e(r,\omega) \equiv \text{sign}\left(\frac{\partial B(r,\omega)}{\partial r}\right) B(r,\omega), \tag{B3}$$

$$r(t) = r + (\Delta r)t \sin\varphi, \quad \omega(t) = (\Delta r)t \cos\varphi.$$

Here, t is a unitless parameter of integration, Δr is a scaling factor that converts t into range units, and $\Delta\omega$ is an equivalent scaling factor for frequency. When $\varphi = 0$, this formula reduces to Eq. (B2) and represents an integration along a possible mainlobe at range r. This incoherent output is now a function of two parameters, source range and integration angle with respect to that range. Theoretically, the normalization factor N will also be a function of range and φ, but experience has shown that N can be treated as constant.

Equation (B3) is a special case of the Radon transform[17,18] which often is found in image processing:

$$\begin{aligned}\Re(p,\varphi,B_e(r,\omega)) &\cong \Re(p,\varphi)|_{r0,\omega 0} \\ &= \int_{-\infty}^{\infty} B_e\left(\frac{p\cos\varphi + t\sin\varphi}{\Delta r}, \frac{p\sin\varphi + t\cos\varphi}{\Delta\omega}\right) dt \Big|_{r0,\omega 0}.\end{aligned} \tag{B4}$$

Here p represents a unitless distance from a reference point $(r0,\omega 0)$ in an image, which is typically the center pixel. Figure B3 provides an illustration of the Radon transform. Given the reference point, the transform outputs image line integrals as a function of both a rotation angle φ around the reference and a displacement p along the rotated axis. Put another way, the line integral is performed along a line perpendicular to this rotated axis and crosses the axis a distance p away from the reference. Therefore, a line lying at an angle φ with respect to the ω axis and passing a minimum distance of p units away from the reference point will be transformed into a point at the coordinates (p,φ).

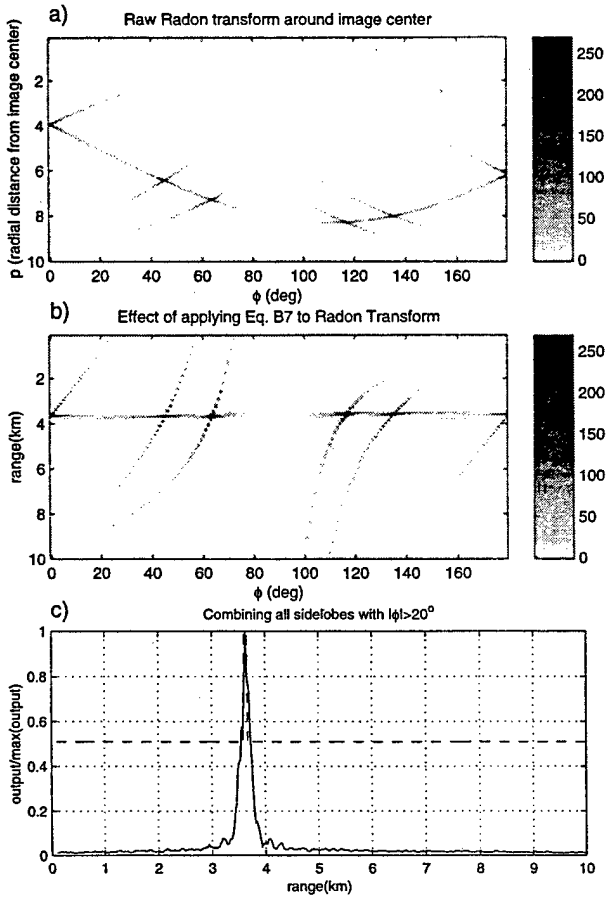

FIG. B4. Demonstration of sidelobe beamforming on the simulated surface shown in Fig. B1(a). (a) Radon transform of the surface performed around the center of the image (5 km, 0). Note that the five lines are now points in the (p,ω) plane. (b) Effect of applying Eq. (B7) to the radon surface. Each point (r,φ) now represents a line integral that intersects the range axis at r, along an angle φ relative to the frequency axis. (c) Effect of averaging the beamformed sidelobes [summing along the φ axis in (b)]. The mainlobe has not been included in the average and the output is normalized by its maximum.

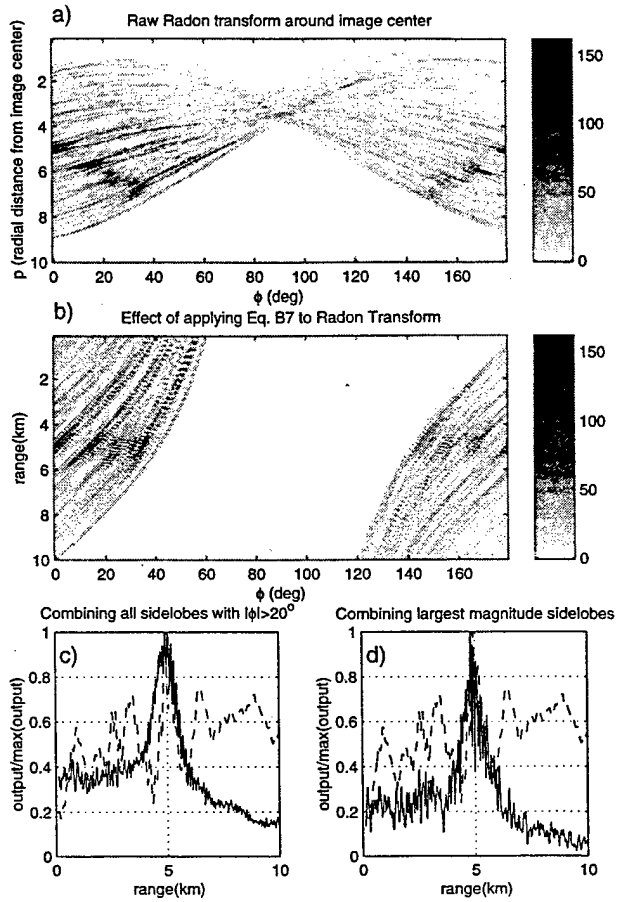

FIG. B5. Demonstration of sidelobe beamforming on backpropagated MFP data. (a) Radon transform of Fig. B2(a). (b) Output of Eq. (37), using transform on (a). (c) Effect of averaging all sidelobe beams with $|\varphi|>20$ degrees (solid line). The incoherent Bartlett result is overlain for comparison (dashed line). Both curves are normalized by their maximum values. (d) Same as (c) but using only sidelobes whose maximum amplitude exceeds a cutoff value. This is an attempt to eliminate angles along which there is no sidelobe energy.

Comparison of Eqs. (B4) and (B3) shows that the sidelobe beamformer can be expressed as a radon transform around the point $(r,0)$:

$$\bar{B}_2(r,\omega)=\|\Re(0,\omega)|_{r,0}\|. \tag{B5}$$

It might appear that if the MFP function has N range bins, then N Radon transforms would have to be conducted, which would be a time consuming process. In practice, only a single transform of the range-frequency plane is required, because a Radon transform produced around one reference point (r,ω) can be related to a transform around another reference point (r',ω') via a "translation theorem:" [17]

$$\Re(p,\varphi)|_{(r',\omega')}=\Re(p-\mathbf{d}\cdot\mathbf{a},\varphi)|_{(r_0,\omega_0)},$$
$$\mathbf{d}=\left(\frac{r'-r_0}{\Delta r},\frac{\omega'-\omega_0}{\Delta\omega}\right),\quad \mathbf{a}=(\cos\varphi,\sin\varphi). \tag{B6}$$

Thus the final expression for the sidelobe beamformer becomes

$$\bar{B}_2(r,\varphi)=\|\Re(p(r,\varphi),\varphi)|_{r_0,\omega_0}\|,$$
$$p(r,\varphi)=\left(\frac{r-r_0}{\Delta r}\right)\cos\varphi+\left(\frac{\omega_0}{\Delta\omega}\right)\sin\varphi. \tag{B7}$$

Figure B4 illustrates this process on the idealized image displayed in Fig. B1(a): The raw Radon transform is shown in Fig. B1(c) where the five lines in the (r,ω) plane have been transformed into the five points in the (p,φ) plane. The reference point for this transform was the center of the image at approximately 5 km and 60 Hz. Applying Eq. (B7) yields the output shown in Fig. B4(b); which shows the convergence ranges of all the sidelobe trajectories. The mainlobe integration is revealed by the bright spot shown near $\varphi=0°$, and the sidelobes by the remaining four points. It is clear that all trajectories converge to 3.75 km. This can be displayed by averaging along the phi axis and plotting the final result in Fig. B4(c). In this case, Fig. B4(c) does not include the mainlobe, which is accomplished by only averaging beams with $|\varphi|>20$ degrees. The mainlobe has been excluded to illustrate that the sidelobes alone contain enough information to obtain the true range.

Figure B5 applies the sidelobe beamformer to Fig. B2(a), using only frequency components greater than 85 Hz. The Radon transform is shown in Fig. B5(a): and the application of Eq. (B7) produces Fig. B5(b). The effects of averaging all beams for $|\varphi|>20$ degrees is shown in Fig. B5(c), and the result of using a more selective average (using only the largest-amplitude beams) is shown in Fig. B5(d). As before, the standard Bartlett average is plotted alongside the new beamformer's output. Clearly the sidelobe beamformer also displays a superior mainlobe sidelobe ratio, at the cost of a broadened peak around the correct range. This broadening seems to occur for two reasons: first, β for shallow-water environments is not exactly one so the sidelobe trajectories will not be exactly straight lines. Second, the peak width produced by a beamformed sidelobe will be on the order of a sidelobe width; which tends to be wider than a mainlobe. The reason for this difference is that the sidelobe is generated by constructive interference between a few modes, while the mainlobe is generated by constructive interference between all modes, including the high-order modes that permit finer resolution.

In summary, the structures contained in the sidelobe trajectories can be incorporated into incoherent sidelobe suppression or sidelobe beamforming algorithms that improve the peak/sidelobe ratio of the final averaged estimator. However, the latter approach only works for modeling shallow-water environments where $\beta-1$, is more computationally intensive, and has a broader peak in range.

[1] S. D. Chuprov, "Interference Structure of a Sound Field in a Layered Ocean," in *Akustika Okeana Sovremennoe Sostoyanie (Ocean Acoustics, Current State)*, edited by L. M. Brekhovskikh and I. B. Andreevoi (Nauka, Moscow, 1982), pp. 71–91.

[2] G. A. Grachev, "Theory of acoustic field invariants in layered waveguide," Acoust. Phys. **39**, 33–35 (1994).

[3] L. M. Brekhovskikh and Y. Lysanov, *Fundamentals of Ocean Acoustics*, 2nd ed. (Springer-Verlag, Berlin, 1991).

[4] A. B. Baggeroer, W. A. Kuperman, and H. Schmidt, "Matched field processing: Source localization in correlated noise as an optimum parameter estimation problem," J. Acoust. Soc. Am. **83**, 571–587 (1988).

[5] F. B. Jensen, W. A. Kuperman, M. B. Porter, and H. Schmidt, *Computational Ocean Acoustics* (American Institute of Physics, New York, 1994).

[6] N. O. Booth, P. A. Baxley, J. A. Rice, P. W. Schey, W. S. Hodgkiss, G. L. D'Spain, and J. J. Murray, "Source localization with broad-band matched-field processing in shallow water," IEEE J. Ocean Eng. **21**, 402–412 (1996).

[7] R. T. Bachman, P. W. Schey, N. O. Booth, and F. J. Ryan, "Geoacoustic databases for matched-field processing: Preliminary results in shallow water off San Diego, California," J. Acoust. Soc. Am. **99**, 2077–2085 (1996).

[8] M. B. Porter, "The KRAKEN normal mode program," SACLANTCEN, Memorandum SM-245, 1991.

[9] A. M. Thode, G. L. D'Spain, and W. A. Kuperman, "Matched-field processing and geoacoustic inversion of blue whale vocalizations," J. Acoust. Soc. Am. (accepted).

[10] W. C. Cummings and P. O. Thompson, "Underwater sounds from the blue whale, *Balaenoptera musculus*," J. Acoust. Soc. Am. **50**, 1193–1198 (1971).

[11] P. Gerstoft, "Inversion of seismoacoustic data using genetic algorithms and a posteriori probability distributions," J. Acoust. Soc. Am. **95**, 770–782 (1994).

[12] P. Gerstoft, "Inversion of acoustic data using a combination of genetic algorithms and the Gauss–Newton approach," J. Acoust. Soc. Am. **97**, 2181–2190 (1995).

[13] P. Gerstoft, "SAGA Users Guide 2.0, an inversion software package," SACLANT Undersea Research Centre SM-333, 1997.

[14] F. D. Tappert, L. Nghiem-Phu, and S. C. Daubin, "Source Localization using PE method," J. Acoust. Soc. Am. Suppl. 1 **78**, 530 (1985).

[15] W. A. Kuperman, W. S. Hodgkiss, H. C. Song, and T. Akal, "Phase conjugation in the ocean: Experimental demonstration of an acoustic time-reversal mirror," J. Acoust. Soc. Am. **103**, 25–40 (1998).

[16] G. L. D'Spain, J. J. Murray, W. S. Hodgkiss, N. O. Booth, and P. W. Schey, "Mirages in shallow water matched field processing," J. Acoust. Soc. Am. **105**, 3245–3265 (1999).

[17] S. R. Deans, *The Radon Transform and Some of its Applications* (Wiley, New York, 1983).

[18] J. R. Fricke and A. B. Baggeroer, "Modal-slowness analysis of plate vibrations," J. Acoust. Soc. Am. **92**, 3228–3238 (1992).

Matched-field processing, geoacoustic inversion, and source signature recovery of blue whale vocalizations

Aaron M. Thode, G. L. D'Spain, and W. A. Kuperman
Marine Physical Laboratory, Scripps Institution of Oceanography, San Diego, California 92093-0205

(Received 28 December 1998; revised 25 October 1999; accepted 27 October 1999)

Matched-field processing (MFP) and global inversion techniques have been applied to vocalizations from four whales recorded on a 48-element tilted vertical array off the Channel Islands in 1996. Global inversions from selected whale calls using as few as eight elements extracted information about the surrounding ocean bottom composition, array shape, and the animal's position. These inversion results were then used to conduct straightforward MFP on other calls. The sediment sound-speed inversion estimates are consistent with those derived from sediment samples collected in the area. In general, most animals swam from the east to west, but one animal remained within ~500 m of its original position over 45 min. All whales vocalized between 10 and 40 m depth. Three acoustic sequences are discussed in detail: the first illustrating a match between an acoustic track and visual sighting, the second tracking two whales to ranges out to 8 km, and the final sequence demonstrating high-resolution dive profiles from an animal that changed its course to avoid the research platform FLIP (floating instrument platform). This last whale displayed an unusual diversity of signals that include three strong frequency-modulated (FM) downsweeps which contain possible signs of an internal resonance. The arrival of this same whale coincided with a sudden change in oceanographic conditions.
[S0001-4966(00)02802-2]

PACS numbers: 43.30.Pc, 43.30.Sf [WA]

INTRODUCTION AND REVIEW OF PREVIOUS WORK

In this paper, matched-field processing[1–3] (MFP) methods have been applied to blue whale (*Balaenoptera musculus*) vocalizations, recorded off the California coast in 1996. The research upon which this work is based is an outgrowth of initial work by the Marine Physical Laboratory to conduct MFP on whales during an unrelated experiment in 1994,[4,5] and to use whale vocalizations for geophysical inversions.[6] The results presented in this paper show how these techniques can obtain high-resolution ranges and depths of blue whale positions out to ranges of 8 km under complex propagation conditions, using as few as eight hydrophones. No previous knowledge of the surrounding ocean bottom was required, because the needed information was extracted from the vocalizations themselves, using global inversion techniques. When combined with the acoustic vector intensity measured from a DIFAR[7] sonobuoy, a three-dimensional localization was achieved. Propagation effects could then be removed from the calls, using the derived locations and inferred ocean bottom properties. This procedure obtained estimates of both the source time signatures and source levels of different vocalization types.

Most localization work on baleen whales has focused on obtaining azimuth and range, usually by employing widely spaced hydrophone assemblies. Recent examples of these approaches are given in Refs. 8–11. Previous depth estimates from cetacean vocalizations have been obtained only under restricted conditions, where the acoustic signal has been assumed to travel directly from the animal to each receiver, allowing standard time-of-arrival methods[12] to be employed. Some examples of this approach have included captive dolphins in a concrete tank,[13] and sperm whales in deep water.[14] However, acoustic signals generated by baleen whales along the coast generally propagate over ranges greater than the local water depth, and they become substantially altered through interaction with the surface and ocean bottom, making the application of standard time-of-arrival methods difficult.[12] The MFP techniques used in this paper have no such limitations; indeed, some signals discussed here have been localized in depth and range to distances greater than 60 times the local water depth, and thus experienced multiple surface reflections and bottom refractions before being recorded. In this case no direct acoustic path between the whale and the receiving array existed.

After a review of the experimental location, geometry, and data analysis procedures in Sec. I, the MFP results are presented in Sec. II A, using data from three distinct acoustic sequences, recorded over a 40-hour time period in 1996 off the northern Channel Islands in the Southern California Bight region. The first sequence (case 1) demonstrates a match between an acoustic track and a visual observation of two blue whales. The next sequence (case 2) demonstrates the maximum ranges obtained from the experiment, covering a 90-min period wherein two different whales are tracked to ranges of several kilometers. The final sequence (case 3) illustrates a high-resolution track of a single whale that swam toward the research platform FLIP, then altered its course to avoid the experiment. This sequence contains three unusual FM signals and three detailed dive profiles.

Section II B compares the sediment properties extracted from the whale vocalizations with those derived from sediment cores taken from the same region. Section II C uses the MFP positions to compute source levels for the animals in cases 2 and 3, and Sec. III D uses multichannel deconvolution techniques[15,16] to strip away propagation effects from three FM sweeps in case 3, demonstrating that the unusual

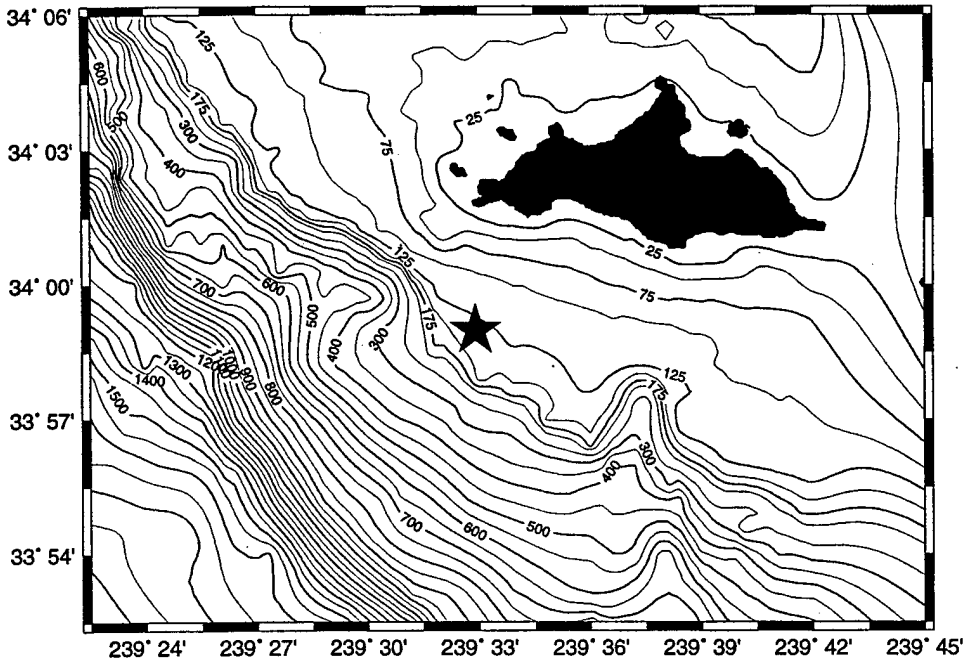

FIG. 1. Bathymetry around the 1996 experiment site. The contour interval is 25 m until 300-m depth, and then increases to 50 m for deeper depths. FLIP location is given by star. Note how the bathymetry to the east and northwest is only mildly range-dependent.

features present in the call are produced within the whale itself, and are not waveguide effects. The discussion in Sec. III discusses whether the unusual FM sweeps in the latter case might indicate an internal resonance, and notes how the presence of this whale coincides with a sudden change in ocean conditions in the area.

The "type A" and "type B" eastern Pacific blue whale vocalizations discussed here are described in greater detail elsewhere.[8–10,17,18] References on blue whale sounds in other regions of the world,[19–25] MFP,[1,2,26,27] and geoacoustic inversion methods,[26,28–34] have also been provided.

I. METHODS

A. Experiment location and geometry

The 1996 experiment was conducted using the research platform FLIP (floating instrument platform)[35] from July 18 through July 22 off the south coast of San Miguel Island, at 33°59′ N, 120°27.221′ W. This location lies within the boundaries of the Channel Islands National Marine Sanctuary,[36] administered by the National Oceanic and Atmospheric Administration. Surveys over the past ten years have observed concentrations of blue, fin, and humpback whales in the region during the summer months. "Whale Habitat and Prey Study (WHAPS)" surveys[37] conducted by the National Marine Fisheries Service, Southwest Fisheries Science Center (SWFSC) have concluded that around 100 blue whales frequent the area each summer. The animals are believed to be feeding off krill, which in turn feed off the plankton blooms growing in the nutrient-rich water upwelling around the islands.[38]

Figure 1 illustrates the bathymetry around the experimental site. The contour maps were constructed using fathometer-corrected data downloaded from the National Oceanographic Service and National Geological Data Center databases. Depending on the tide level, the water depth at the experiment site varied between 129 and 133 m. The vocalizations presented here will be from animals swimming from the E to SE of FLIP, a region where the water depth changes by only 30 m over 10 km.

The experimental deployment is illustrated in Fig. 2, and consisted of a 48-element[39] vertical array with a hydrophone spacing of 1.875 m, sampled at a rate of 1500 Hz. A General Oceanics inclinometer was attached 1.7 m above the shallowest hydrophone element, and recorded the array tilt magnitude and direction, inclinometer depth, and water temperature every 90 sec. Data from the vertical array were used to conduct the MFP, while information from both the vertical array tilt and an occasional DIFAR sonobuoy[7] estimated

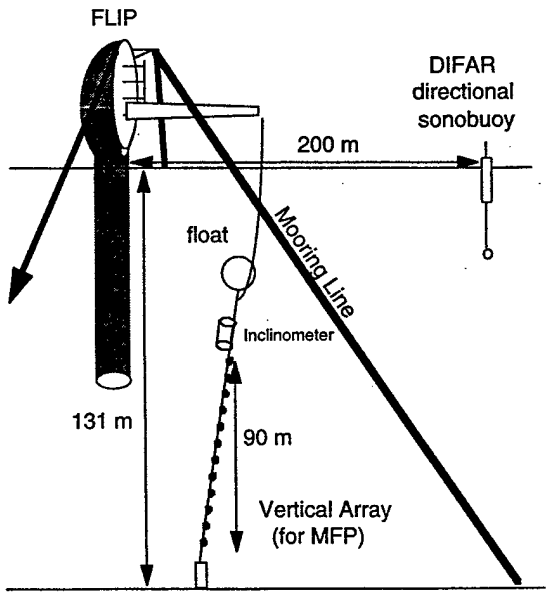

FIG. 2. Experimental setup of the MFP experiment. The vertical array is used to compute range and depth of calling animals. Source azimuth could occasionally be estimated by using either a DIFAR directional sonobuoy (as in case 2), or by taking advantage of the vertical array tilt caused by strong currents in the area (Sec. I C). The thick dark lines represent mooring lines.

source azimuth,[40,41] thus yielding a three-dimensional location. Subsequent work showed that localization could be accomplished using as few as eight hydrophones as long as they spanned 90 m of vertical aperture.

B. Data analysis and inversion procedures

Traditional MFP requires information about the ocean depth, bottom composition, sound-speed profile, and tilt of the vertical array, in order to construct an accurate model of the acoustic field received at the area. Bathymetry information was independently available, but the other environmental information was sparse or unknown. The analysis for each case presented in Sec. II began by selecting several large signal-to-noise ratio (SNR) calls throughout the sequence for "focalization" or inversion. By applying a genetic algorithm[42,43] inversion software package[34] to a normal-mode numerical model,[44] the required environmental parameters were extracted from the vocalizations themselves, while simultaneously recovering the best-fit range and depth of the whale. The fitness criteria used were the normalized output of the Bartlett processor, incoherently averaged over 3–10 frequencies between 16 and 130 Hz. Identical global optimization procedures were used for each inversion, which adjusted 18 parameters in an attempt to maximize the peak correlation of the incoherently frequency-averaged ambiguity surfaces. Each inversion was repeated 40 times for each vocalization sample, using a different initial population of trial solutions, and the inversion run that yielded the largest correlation was retained.

Nine of the 18 inverted parameters defined a geoacoustic model of the ocean bottom that assumed a sediment layer overlaying an infinite basement layer. The sediment thickness was set to 70 m, deeper than the expected bottom penetration for all frequencies except possibly 17 Hz. A sediment sound-speed profile was constructed by allowing the inversion to adjust the sediment sound-speed at depths of 23, 46, and 70 m beneath the water/sediment interface, as well as the bottom half-space sound-speed. The sediment sound-speed at the water/sediment interface was allowed to vary between realistic values of 1450 and 4000 m/s, and the sound-speed was allowed to increase between 0 and 1000 m/s every 23 m, ensuring the physically realistic result that the bottom velocity would increase with depth. The inversions did not solve for possible large shear speeds in either the sediment layer or half-space, as the normal-mode models used for the inversion incorporated a perturbation approach to compute shear, which is valid only for small shear values.[2]

Baseline water-borne sound-speed profiles were constructed using temperature data from five XBT casts. The technique of empirical orthogonal functions (EOFs) was applied to enable inversion of the water column sound-speed profile using only a few parameters.[45] The MFP results were insensitive to the exact shape of the sound-speed profile used. The inversion techniques were benchmarked by performing inversions on the Swellex-3[27] data set, where the geoacoustic parameters were already known.

Once acquired, the inversion parameters were used to perform MFP on the rest of the calls in the sequence, while ensuring that updated "snapshots" of the vertical array geometry were used. Once a time series was selected, a single global inversion typically took 10–20 min using a Sun Ultra workstation. A MFP computation using the inversion results took 30–60 sec per call, using routines developed in MATLAB.

C. Interpreting inverted array tilt

Imagine a tilted vertical array with a total offset H between the top and bottom hydrophones. Because MFP models the two-dimensional acoustic field between the source and receiver, it is only the projection (H') of the total offset onto the MFP plane that influences the received acoustic field. If the source bearing is the same as the tilt direction, then $H' = H$; if the source bearing is perpendicular to the tilt bearing, then $H' = 0$—the projected offset is zero. Because the maximum array tilt and tilt direction were independently measured by an inclinometer, the projected offset can be converted into a rough source bearing estimate. The convention used in this paper is that a negative value of H' indicates the array is tilting away from the source. One important consequence of this behavior is that if the projected array tilt remains constant over time while the range decreases, then the source must be moving toward the array.

II. RESULTS

In this paper all dB units have been expressed in terms of pressure spectral density (*re* 1 μPa^2/Hz), and source levels in terms of source pressure level spectral density (*re* 1 μPa^2/Hz @ 1 m).

A. MFP tracks

1. Case 1—demonstration of an acoustic/visual match

The ocean conditions were calm over the 15-min period shown in Fig. 3, beginning at 14:01 GMT, Julian Day 204, 1996, and are among the last calls recorded during the experiment. The myriad 20–30-Hz pulses that are prominent around 750 sec may be fin whale calls.[46–48] In addition, at least three blue whales are vocalizing during this time, generating two types of signals known to be produced by blue whales.[9,17,18,20,49,50] The broadband pulsed call is conventionally called "type A," and the harmonic FM sweep is labeled "type B." One animal is producing very faint B calls (~100 dB *re* 1 μPa^2/Hz), with only the 50-Hz tone visible, suggesting that it is greater than 5 km away. Another animal generated the two A-B sequences that begin at roughly 100 and 310 sec along the time axis in Fig. 3. A third animal has produced the intense broadband type A calls recorded at 293, 505, and 718 sec (labeled "a," "b," and "c" in the figure), and these calls are the focus of this case. Of the three calls, the 505-sec call has the best signal-to-noise ratio. The 293-sec call is also of good quality, but the 718-sec signal suffers from contamination from pulsing broadband noise and possible fin whale pulses.

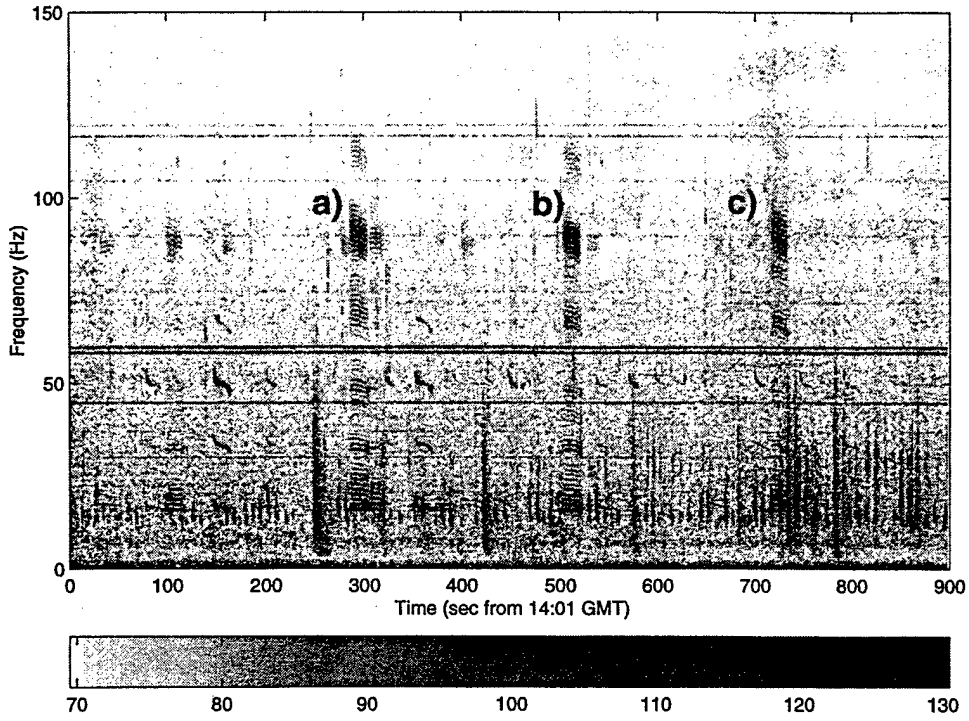

FIG. 3. Spectrogram of case 1, Julian Day 204 time sequence, starting at 14:01 GMT. Power spectral density levels are in units of dB *re* 1 μPa^2/Hz. Note the three strong type A calls at 290 ("a"), 505 ("b"), and 720 ("c") seconds. The multiple vertical energy bands between 20 and 30 Hz may be fin whale vocalizations.

The inversion procedure was performed on each of the three high-level type A calls, using an incoherent average of 8–10 frequencies between 16 and 112 Hz. The inversion results are graphically displayed in Fig. 4. The inverted sediment sound-speed profiles from the three calls are generally consistent to within ± 50 m/s down to depths of 46 m beneath the surface, with a mean speed around 1621 m/s at the water sediment interface. The accuracy of these geophysical estimates is explored further in Sec. II B.

The multiple arrival paths from a propagating acoustic signal generate an interference pattern in the received pressure field along the array, as a function of depth. To compare the received data from the "b" call with that of the best-fit model, the measured vs modeled pressure magnitude across the vertical aperture of the array is plotted in Fig. 5, for six different frequency components. The fit is excellent across a wide range of frequencies, particularly in the high signal-to-noise (SNR) ratio band between 85 and 95 Hz.

The frequency-averaged ambiguity surfaces for each call are displayed in Fig. 6, using the adaptive white-noise constraint (WNC) MFP processor,[51,52] where the constraint has been set to 3 dB below the maximum white-noise gain. The WNC correlation output is generally less than that of the Bartlett processor.

Clues about the whale's azimuthal position are provided by the projected array geometry obtained from the inver-

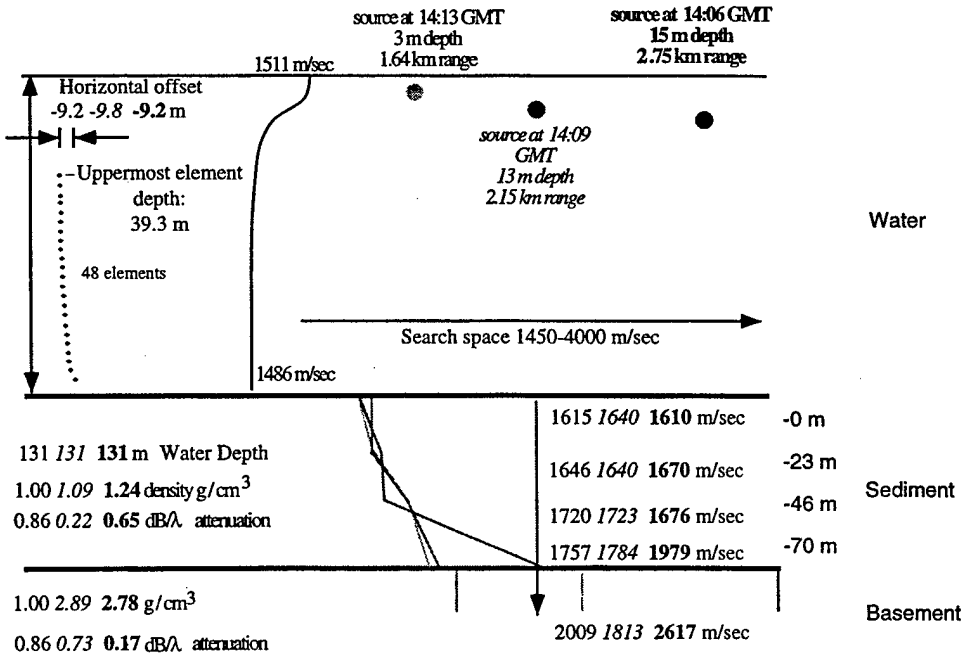

FIG. 4. Illustration of best-fit inversion model for the three type A calls from case 1. Parameters obtained from the same call share the same shading and text style.

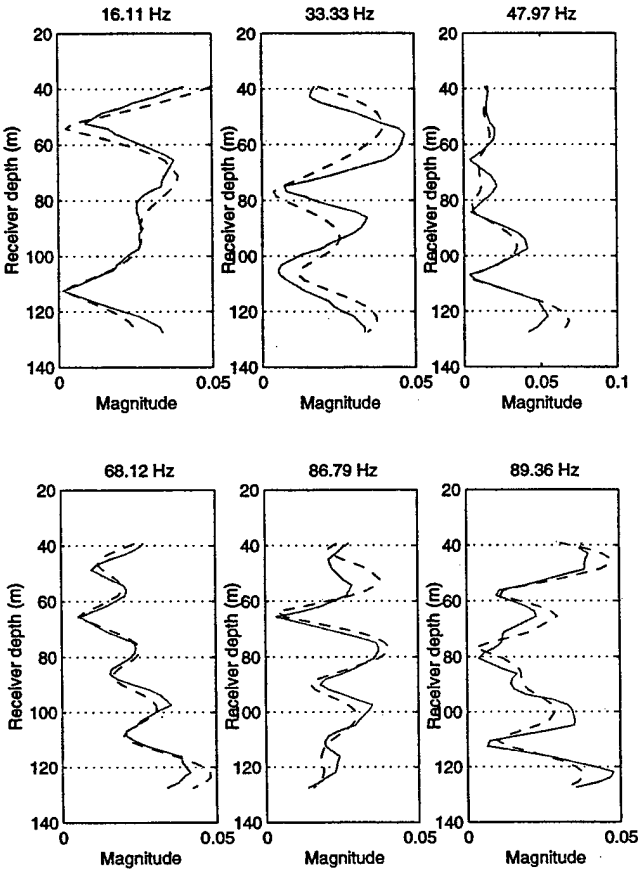

FIG. 5. Comparison between the normalized sound pressure magnitude from the middle type A call (dotted line), and that predicted by the best-fit inversion, as a function of depth for six different frequency components.

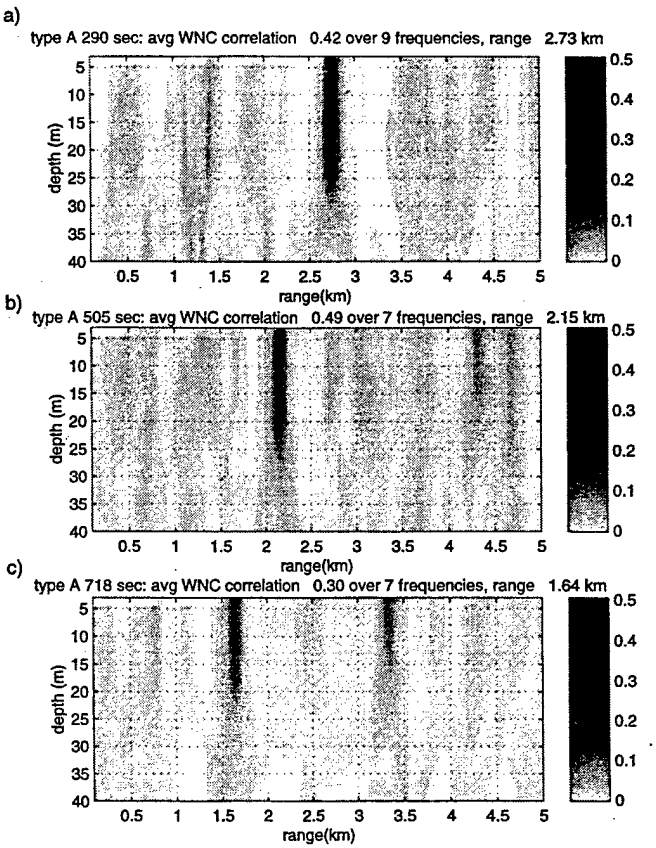

FIG. 6. Ambiguity surfaces from case 1 calls shown in Fig. 3, using the white-noise constraint (WNC) processor. The constraint has been set to 3 dB below the maximum white-noise gain. Frequencies have been selected from the 32-, 48-, 65-, 90-, and 112-Hz bands. Generally correlation values of the WNC are lower than Bartlett values. (a) 290-sec call, average of nine frequencies between 17 and 112 Hz; (b) 505-sec call, average of seven frequencies between 17 and 112 Hz; (c) 720-sec call, average of seven frequencies between 17 and 112 Hz.

sions. For example, the projected horizontal offset H' between the top and bottom hydrophone remained constant at about -9.5 m, so the whale must have been swimming along a radial directly toward FLIP. Had the bearing of the animal relative to FLIP changed significantly during the calling sequence, the inverted array tilt would have changed with time. The negative tilt values indicate the array was tilting away from the whale, and since the array was tilting toward the NW, the bearing of the animal must be to the E or SE. The whale moved 1.1 km over about 430 sec. Its average speed over this time was therefore 2.6 m/s (9.2 km/hr), consistent with estimated swimming speeds between 5 to 33 km/hr for blue whales.[53]

Given the long duration of these calls (around 15 sec), it is possible to perform MFP on sequential time segments within a call, obtaining the animal's dive profile while vocalizing. The ranges and depths from the resulting ambiguity surface mainlobes are plotted in Fig. 7, at 1-sec intervals, for the 505-sec ("b") call. While calling, the animal's range decreases by 2.5 to 3 m/s, consistent with the long-term swimming speed derived from Fig. 6.

The animal seems to remain at a constant depth over the duration of the 505-sec call, to within the resolution of the MFP processor. This theoretical resolution limit, based on the Cramer–Rao lower bound,[3] is expected to be around ± 2 m in depth and ± 10 m in range, for a 89-Hz signal with a 20-dB signal-to-noise ratio (SNR). Bathymetry mismatch also introduces a depth uncertainty, as the true ocean bottom is not flat. At 2.1-km range, the water depth lies between 110 and 150 m, depending on the azimuth used, which translates into an absolute source depth uncertainty of about ± 3 m[54] and a range uncertainty of about 15%. Thus the relative ranges and depths in Figs. 6 and 7 are probably accurate, but the absolute ranges and depths have uncertainties of ± 3 m in depth and ± 300 m in range.

Both Figs. 6 and 7 suggest a swimming speed of 2.6 m/s toward FLIP. Therefore this whale would have taken about 10.5 min to cover the remaining 1.6 km to the vertical array, suggesting that a visual sighting of an animal from FLIP should have been noted between 14:23 and 14:24 GMT on Julian Day 204. Indeed, this was the case.

Beginning at 14:23 GMT, a videotape of two whales approaching FLIP was recorded using a Cannon Hi 8-mm ES5000 camcorder. During this period, the animals approached from the E/SE, performed a shallow dive (about 30 m away from FLIP), then altered course slightly to swim away to the NW. Scientists at Southwest Fisheries Science Center identified both animals on the videotape as blue whales.[55] If these whales were indeed responsible for the recorded calls, then it seems likely that only one of them vocalized, due to the consistency in style and timing of the

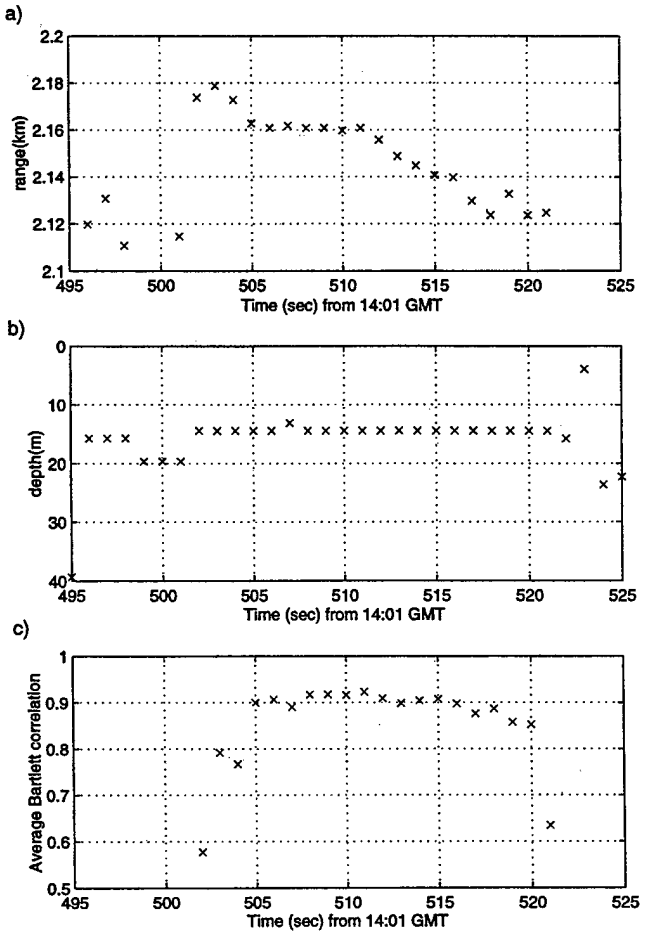

FIG. 7. Estimated changes in (a) range and (b) depth during "b" type A vocalization. Seven frequencies between 30 and 120 Hz were used in the MFP processing. Plot (c) shows the average correlation of the MFP peak over time. Estimated Cramer–Rao bound resolution is ±3 m in absolute depth, ±10 m in absolute range.

type A calls. One animal was somewhat smaller than the other, so perhaps the pair was a mother and her calf—but this will remain a speculation.

2. Case 2—maximum ranges obtained from MFP

The 90-min sequence analyzed here, beginning at 19:52 GMT on Julian Day 203, demonstrates for the first time how MFP can track calling whales to ranges in excess of 60 water depths, a situation where no direct path between the source and receiver exists. While case 1 analyzed three type A calls over a 15-min period, case 2 contains data from 67 type B and 39 type A calls from two different animals, one out to a range of over 8 km. Azimuthal information provided by a DIFAR sonobuoy was also available during part of the sequence, enabling high-resolution three-dimensional position estimates.

At first, only a single whale called, making type A-B doublet patterns. At approximately 20:36 GMT (44 min into the sequence), a second whale began calling. This animal had a different vocalization pattern, making three to five B calls for every pulsed A call. Both whales called at predictable intervals, and both also had their own characteristic FM downsweeps, making it easy to separate individuals from the spectrograms. For 30 min both animals called simultaneously, before the first whale fell silent at around 21:07 GMT (75 min into the sequence). Fortunately, a DIFAR sonobuoy had begun recording data 5 min earlier, and so precise azimuthal estimates were obtained for both animals. The second animal continued calling for another 15 min before suddenly lapsing into silence shortly past 21:22 GMT. Signal harmonics as high as 135 Hz were detected during this whale's final vocalizations.

Several strong type B calls produced by the second whale around 21:20 GMT (88 min into the sequence) provided excellent inversion sources, due to their high SNR and the presence of many harmonics. The resultant range and depth tracks from both animals, assuming a range-independent bathymetry, are plotted in Fig. 8(a) and (b). Only the 32-, 50-, and 65-Hz frequency bands have been averaged to generate these plots, because they were the only components present in all calls. Incorporating the higher-frequency components, whenever they were present, did not significantly alter these results. Each data point represents a covariance matrix constructed from 4096 pts (2.4 sec) of data. Adjacent data points were spaced 1 sec apart, so a single call yielded 10 to 15 range/depth estimates. Only points whose frequency-averaged peak correlation was greater than 0.7 have been plotted. Because of the higher SNR of the type B tones, the correlations of the type B calls are generally better than the type A estimates.

The first whale was detected at nearly 9-km range, which steadily decreased at a rate of about 8.2 km/hr, again consistent with known swimming speeds. The depth estimates show high scatter until the range became less than 5 km, and then they settle to values between 20 and 30 m. This animal swam within 1.4 km of FLIP at its closet point of approach.

The second whale's behavior provides an interesting contrast, in that its range remained relatively constant over 45 min. Gaps in vocalization are visible, which probably occurred when the animal surfaced. When first detected, the whale's apparent depth was shallow, at around 10 m. Over the next 10 min the source depths increased to a final average value of 20 m, where it remained for the rest of the sequence.

Figure 8(c) shows the best-fit projected array offsets (H') from 17 global inversions, computed at various times from both animals. As discussed in Sec. II C, projected array tilts can be converted to azimuthal estimates if assumptions about the array geometry are made. Because the array was tilting toward the west, the initial negative array offsets indicate that both animals were first detected roughly east of FLIP. The second whale's projected tilt remains fixed between −24 to −26 m, suggesting that its bearing did not change much over this time. By contrast, the azimuth of the first whale changes considerably, as the projected offset shifts from −25 to +25 m over 90 min. If the total array offset is assumed to lie between 25 and 30 m, then both whales were first detected at a bearing of around 95°, almost due east of FLIP. The first (transiting) whale reached its closest approach to FLIP at roughly 330° bearing, and stopped calling at approximately 315° bearing. The second whale, whose apparent bearing never changed, had a final estimated bearing of 105±40°. The DIFAR results from this

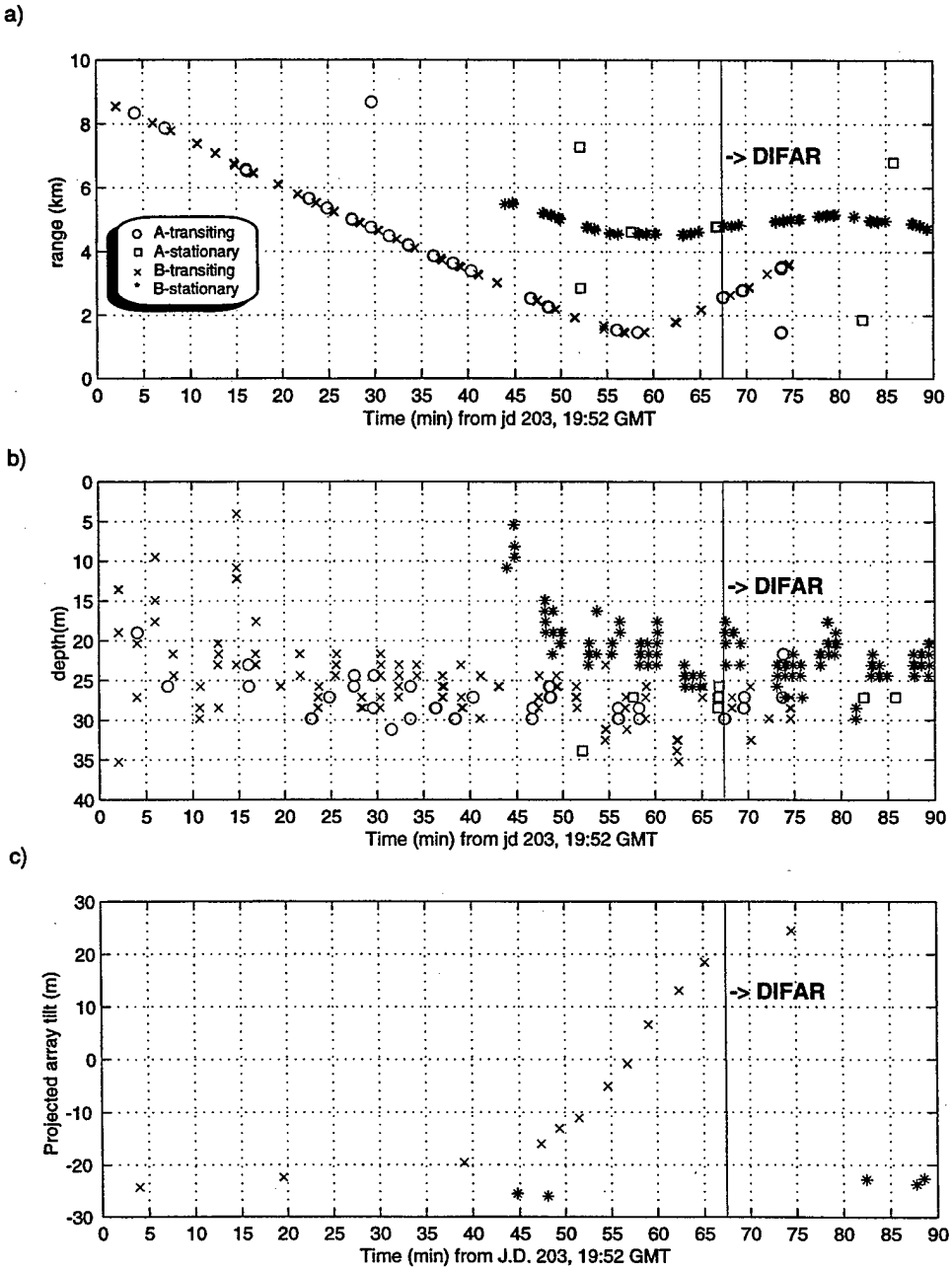

FIG. 8. Computed ranges and depths from case 2, for two animals over 90 min, starting from 19:52 GMT on J.D. 203. The 32-, 50-, and 65-Hz frequency bands were used in the MPF processing, assuming a range-independent bathymetry. A DIFAR sonobuoy begins recording data at 21:01 GMT. Each data point represents 2.5 sec of data, spaced 1 sec apart within a call. (a) range versus time; (b) depth versus time; (c) inverted horizontal array offset versus time. Whale bearing can be estimated from array offset.

time confirmed the second whale was calling from a bearing of 105°, and that the final bearing of the transiting whale was 340°. Both measurements thus agree with the rough inverted-array tilt predictions.

Because the azimuths of these calls were available, the effects of incorporating a more accurate bathymetric profile could be evaluated. For example, the true bathymetry along a 105° bearing from FLIP changes from 133 to 118 m over 5 km. When range-dependent replicas were recomputed using a parabolic-equation model,[56] the second whale's range estimate became 4.6 km, instead of the 5-km range obtained from assuming a flat bottom. The estimated depth also became about 2 m shallower, in agreement with theoretical expectations.[54] The effects of range-dependent bathymetry were therefore concluded to be mild for animals approaching from the east, or for animals less than 3 km away from FLIP.

3. Case 3—close approach with unusual vocal behavior

Case 3, the hour-long sequence analyzed here, began with a single type A-B doublet recorded on Julian Day 204, 1996, at 8:30 GMT. After a 10-min gap, two strong bouts of unusual calls appeared, lasting about 14 min. These vocalization bouts were striking in their variety. Each FM sweep had a different modulation, from straightforward downsweeps to U-shaped contours. The animal switched between type A-B doublets and type A calls followed by multiple Bs.

Between 29 and 30 min, the whale generated several heavily modulated type B calls and two unusual FM ("type D^{10}") sweeps, which are plotted in Fig. 9(a). The whale made a third type D call around 100 sec later, then continued calling before lapsing into another 6-min period of silence beginning around 34 min. At 40 min, the animal generated

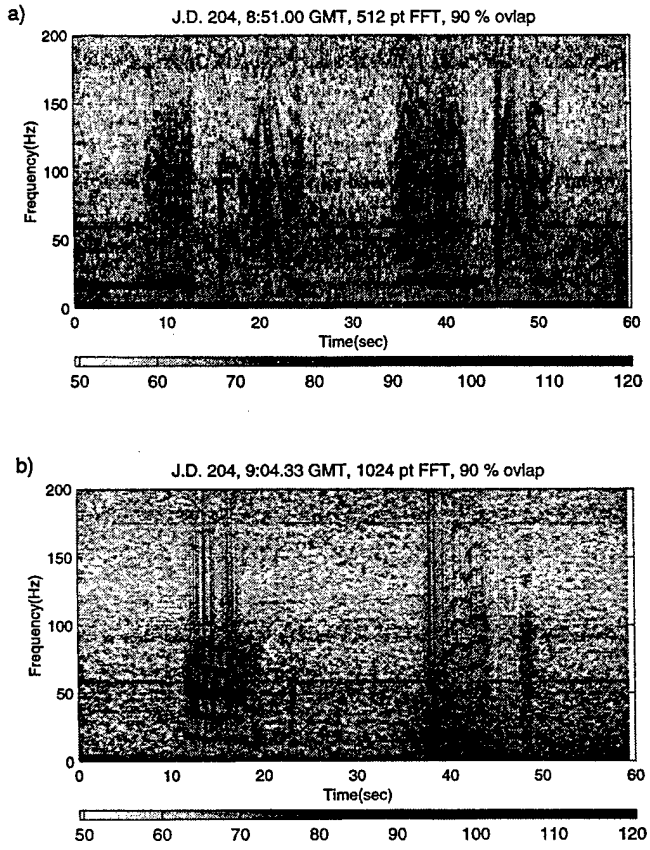

FIG. 9. Spectrograms of 60-sec segments of unusual calls recorded during case 3, expressed in units of pressure spectral density (dB *re* 1 $\mu Pa^2/Hz$ @ 1 m). Both sets of calls were produced when the animal was near the bottom of its dive profile: (a) Strongly modulated type B and D downsweeps, beginning at 8:51 GMT; (b) other examples of highly modulated calls, beginning at 9:04:30 GMT.

two more bouts of vocalizations, separated by an apparent breathing gap at 45.5 min. Some examples of calls generated over a 1-min period during the last bout are shown in Fig. 9(b). The whale finally fell silent at 55 min, or 9:17 GMT.

Figure 10 shows the final MFP results for this track, assuming a flat bathymetry. As with Fig. 8, the results displayed here use frequency components picked from the 32-, 50-, and 60-Hz bands, each point represents an analysis of 2.4 sec of data, and adjacent points are spaced 1 sec apart. By using only these three frequency components, all calls could be included. Using higher-frequency components, when available, did not change the localization estimates.

Figure 10(a) shows the isolated type A-B doublet was generated at around 3 km range, at around 30-m depth. The first strong vocalization bout started at 1.67-km range, which steadily decreased at an average rate of 1.5 m/s to a minimum range of 386 m, after which the whale ceased calling. After the 6 min gap, the animal produced two more calling bouts, both showing the animal's range now increasing. The animal's radial velocity seemed to increase from 0.58 to 1.23 m/s between the two bouts. The last fix on the animal yielded a range of 1.24 km, after which it fell silent.

The depth estimates in Fig. 10(b) show four complete dive profiles. The scatter of adjacent data points (± 4 m) is consistent with theoretical predictions at these frequencies and ranges. Generally, the animal began calling at 20-m depth, and over 2–3 min descended to a depth of 30 to 35 m. After holding this depth for another 2–3 min, the animal began ascending while continuing to vocalize. The final calls were made between 15- to 20-m depth, with an estimated depth resolution of ± 5 m. The animal took about 2 min to surface and breathe, before descending for the next calling bout.

Figure 10(c) shows the inverted projected array offsets of the vertical array. The projected array tilt remained constant at -10 m as the animal approached FLIP, except for a small excursion at 20 min. At this time the array was leaning WNW, so the animal must have arrived from an easterly bearing, similar to those obtained in the previous sections. The constant projected tilt indicated the animal was swimming directly toward FLIP, just like the two whales in case 1. After the 6-min calling gap, the third calling bout produced a projected array tilt of 0, indicating that the animal had veered off to the side of FLIP, increasing its range to 490 m. The increasing positive tilt values following this time suggest that the animal had swum past FLIP, steadily changing its bearing with respect to FLIP, and thus swimming along a different route than its earlier approach.

Separate estimates of the whale's bearing were obtained by converting the projected array tilt into a bearing estimate (Sec. I C), and by using range-dependent MFP runs to obtain the best-fit bathymetry profile between FLIP and the whale, which can be converted into a bearing estimate.[57] The combined analyses suggest the whale arrived from a bearing between 80 and 120°, while swimming directly toward FLIP to within a range of 390 m. The animal then veered to the north, and may have swum a partial circle around FLIP, before finally swimming toward 340–350°. Thus the initial and final bearings of this whale are similar to those obtained from the transiting whale in case 2. However, this whale clearly made a course correction to avoid FLIP.

B. Evaluation of geoacoustic inversion results

This section summarizes the results from the 48 geophysical inversions extracted from the whale vocalizations discussed in cases 1–3, and compares the estimated sediment speeds with those expected from core samples collected from the region. Most inversions used type B calls, due to their high SNR ratio. Each inversion also optimized the waterborne sound-speed profile, but the results were relatively insensitive to the details of the profile shape. The low frequencies used in the inversion were probably the reason for this insensitivity; for frequencies greater than 150 Hz, the sound-speed profile structure should have more influence on the vertical field structure.

The most important geoacoustic inversion parameters were the sediment sound-speeds at the water/sediment interface, and at depths of 23, 46, and 70 m beneath this interface. The inversion also solved for the best-fit sediment density and attenuation, and for the speed, density, and attenuation of the acoustic half-space that was assumed to lie beneath the sediment. The half-space properties will be ignored here, because the acoustic field energy was not expected to penetrate deeper than 70 m. The inversion results confirmed this ex-

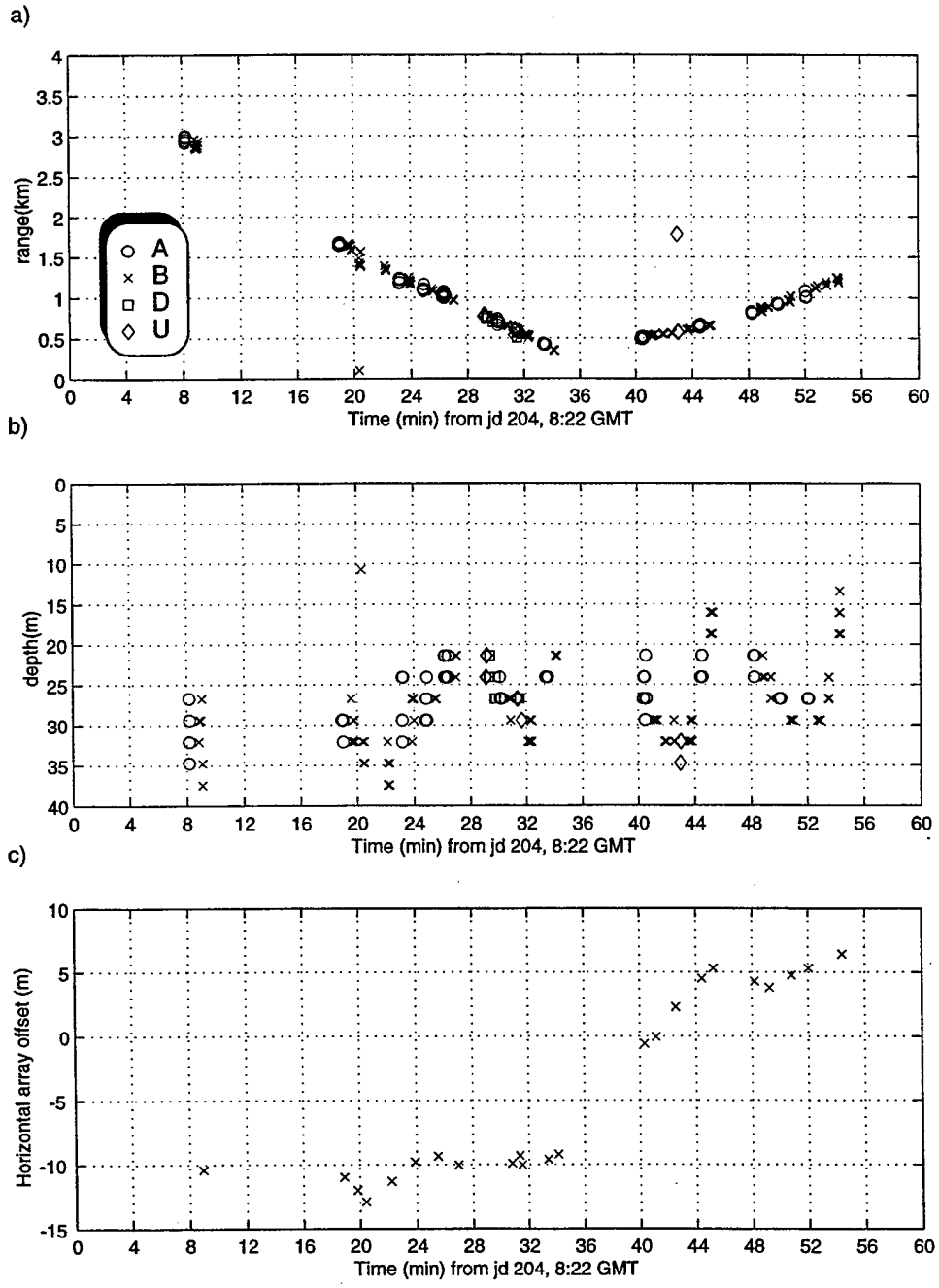

FIG. 10. MFP track of case 3. The track was generated using the 34-, 50-, and 67-Hz signal components, assuming a range-independent bathymetry. Each data point represents 2.5 sec of data, spaced 1 sec apart. The "U" label represents highly modulated type B calls. (a) Blue whale range; (b) blue whale depth; (c) projected horizontal array offset estimated from global inversions.

pectation: the inverted half-space parameters were essentially randomly distributed.

The inversions assumed sediment properties were not a function of source location. In reality the bottom was heterogeneous, so the results presented here represented a range-averaged estimate of the bottom properties between each source and FLIP.

Figure 11 displays the inverted interface sediment sound-speeds as both a function of range from FLIP and the whale used as the inversion source. As discussed previously, the precise azimuths of the calling whales were difficult to determine, except when DIFAR sonobuoy data were available. However, each inversion indicated whether a particular call arrived from the east or west, by combining the projected array tilt with knowledge of the array tilt direction. Figure 11 incorporates this information by plotting easterly data as negative ranges, and westerly data as positive ranges.

This sound-speed parameter was allowed to vary between 1450 m/s (representative of water-saturated mud) and 4000 m/s (typical basalt values) during the inversions. Despite this wide range, all inversion results lie between 1550 and 1800 m/s, with 75% lying between 1600 and 1700 m/s, or 4% of the allowed search space. These values are associated with silty/sandy bottoms.[58] Inversions obtained from the same animal over a small range interval also yielded consistent results; the scatter of these adjacent inversion points is about ± 25 m/s. The scatter is much larger between different cases at similar ranges, because the animals are probably calling from different bearings, and the acoustic energy is sampling different sediment profiles. There was no obvious correlation between the spread of the results and the number of frequencies used in the inversion. One might have ex-

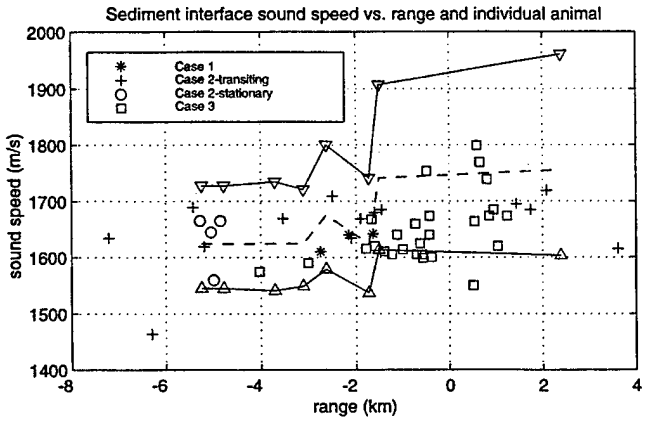

FIG. 11. Inversion results for sediment interface speed, as a function of inversion range and whales used as the acoustic source. The dashed line shows the sound-speeds derived from sediment core mean grain sizes. The solid lines show the sound-speeds computed from grain sizes one standard deviation from the mean. Triangles indicate the ranges of the core samples from FLIP. Negative ranges represent locations east of FLIP, and positive ranges are to the west. The "stationary" whale mentioned in the legend refers to the animal in case 2 that held its bearing fixed at a steady range of about 5 km.

pected the precision to increase as higher-frequency components are included; however, higher frequencies also penetrate less deeply into the sediment, and thus involve a different spatial average.

The recovered surface sediment speed is the only geoacoustic parameter for which independent information exists, in the form of sediment cores collected in the region by various institutions, particularly the United States Geological Survey (USGS) and the University of Southern California (USC)[59] over the past several decades. The penetration depth of these cores is generally less than a meter.

The sediment core data report the grain size distribution using a logarithmic measure $\varphi = \log_2$ (grain size in mm). Considerable variation exists in the particle sizes within a particular sample, so both the mean and standard deviation of φ are recorded. Sediment grain sizes can be converted to bottom sound-speed estimates via an empirical fit,[60] using a measured water sound-speed of 1485 m/s. Three sediment sample speeds are plotted in Fig. 11. The dashed line uses the mean φ, and the two solid lines use φ values lying one standard deviation on either side of the mean. The triangles indicate the ranges of the individual cores from the FLIP position. The plotted core data are restricted to those obtained within 8 km of FLIP, in water depths between 100 and 200 m. The reason for restricting the water depth is that there is a correlation between water depth and sediment sound-speed. For example, as the water shallows while approaching San Miguel shore, both the particle size and sediment sound-speed increase. Even with this depth restriction, the sediment sound-speed apparently changes west of FLIP. Part of this change may reflect the fact that only one core is available west of FLIP (for some reason a gap in sampling occurs to the west in an otherwise well-covered area).

East of FLIP, the whale inversion data lie within ± 50 m/s of the average sediment core sound-speed. The inversions underestimate the mean sound-speed between -1 and $+4$ km range, but this comparison is based on only two sediment cores. In general, the inversion results show a good match with the limited ground truth information available, particularly considering that the animals' bearings are imperfectly known.

Table I summarizes the properties and locations of the sediment cores used in this section. The "AHF#" column refers to the indexing system used by USC to record their samples.

C. Source level estimates

Using the range and depth information in Figs. 8 and 10, multichannel deconvolution techniques[15,16,61] were applied to estimate the source levels of the harmonic frequencies for the three whales in cases 2 and 3. Because the whales' acoustic power output varied considerably during a single vocalization, it is necessary to perform multiple estimates per call to estimate the maximum source levels.

Figure 12 displays the source spectral density levels (dB *re* 1 μPa^2/Hz @ 1 m) for the five lowest-frequency harmonics of the whales in case 2. To convert spectral densities into tonal spectral level, 4 dB should be subtracted from these values (to account for the 0.4-Hz frequency bin width). The uncertainty in these estimates are about ± 5 dB.

Some interesting results are that the 50-Hz tone source level is within 5 dB of the 17-Hz tone level, and that both animals consistently maintain a maximum source spectral density level of about 185 dB *re* 1 μPa^2/Hz @ 1 m (thus total power between 10–100 Hz is about 180 dB *re* 1 μPa @ 1

TABLE I. Sediment core interface sound-speed estimates, based on a water sound-speed of 1485 m/s.

AHF#	Latitude	Longitude	Range (km) from FLIP	Water depth (m)	φ	Skewness	Expected sound-speed (m/sec) over ± 1 standard deviation: Min.	Mean	Max.
24237	33.97	120.45	1.51	169	2.3 ± 2.1	1.3	1613	1741	1907
24238	33.967	120.433	2.63	135	3.3 ± 1.8	2	1579	1676	1741
24239	33.968	120.418	3.71	128	4.2 ± 1.8		1540	1624	1735
23159	33.983	120.435	1.73	115	4.2 ± 1.9	2	1537	1624	1742
23163	33.983	120.42	3.11	107	4.2 ± 1.6	6.5	1548	1624	1721
23164	33.985	120.402	4.78	100	4.2 ± 1.6		1548	1624	1727
23184	33.968	120.400	5.24	115	4.2 ± 1.7	2.5	1544	1624	1728
25192	34.00	120.47	2.39	110	2.1 ± 2.5	0.5	1608	1761	1968
FLIP	33.98	120.454		130					

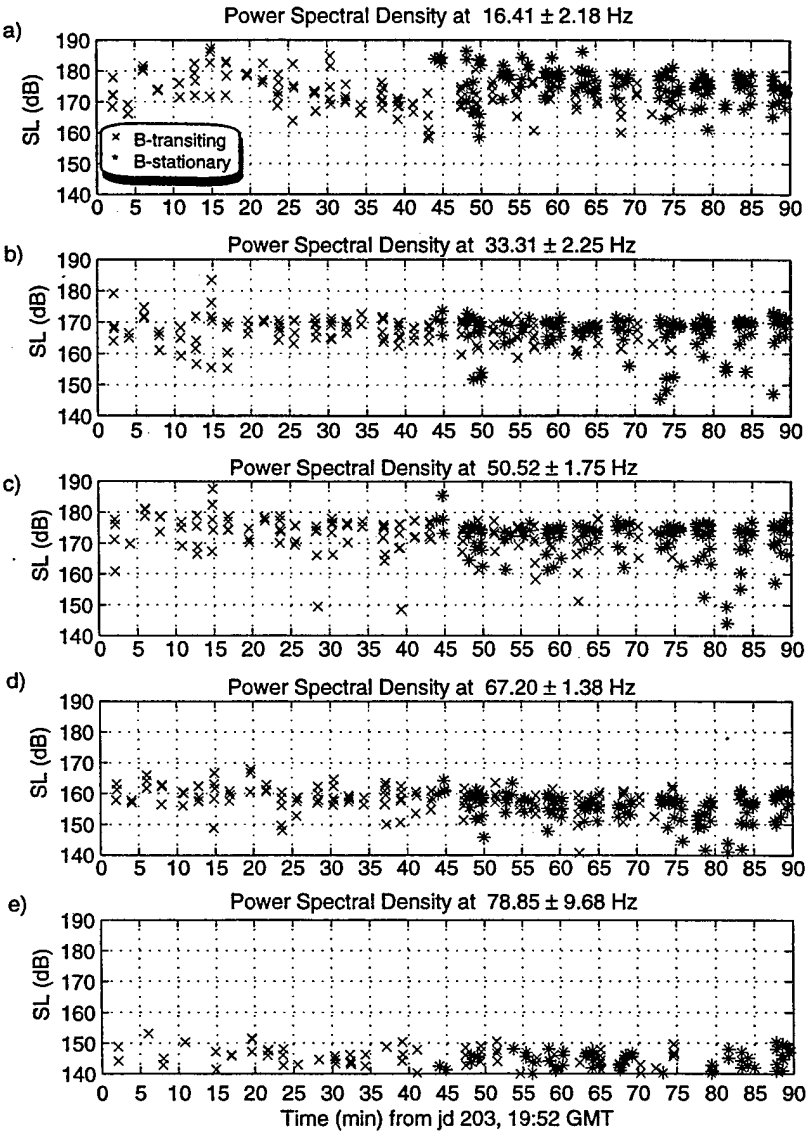

FIG. 12. Blue whale type B call source levels for case 2, estimated using locations given in Fig. 8. Levels are given in terms of pressure spectral density (dB *re* 1 μPa^2/Hz @ 1 m). (a) 16-Hz band; (b) 32-Hz band; (c) 51-Hz band; (d) 67-Hz band; (e) 79-Hz band.

m). In addition, 43 min into the sequence both animals were calling within 2 km of each other, yet neither animal appeared to alter its movements or vocalization patterns in response to the other's presence.

The source levels estimated from case 3 are plotted in Fig. 13. The 17-Hz tones are surprisingly weak, reaching a typical spectral density level of only 160–170 dB *re* μPa^2/Hz @ 1 m, around 10 dB weaker than the levels plotted in Fig. 12. However, the source levels of the harmonics are similar for both cases.

D. Source signature recovery for case 3

Precise knowledge of a blue whale's acoustic location allows not only the source levels to be recovered, but also the relative phase between frequency components of a call. Thus the original time series produced by the whale can be estimated, using multichannel deconvolution methods.[15,16,61]

During its final dive before passing FLIP, this whale generated three strong "type D" FM downsweeps,[10] plotted in Fig. 9(a). Single-element spectrograms of these signals revealed interesting narrow-band regions of high intensity levels between 60 and 120 Hz. To verify that these regions were not products of waveguide propagation effects, as might be reasonably expected,[62] the source time signatures were estimated for the three calls using a Gauss–Markov estimate [Eq. (4) in Ref. 15]. Calibrated spectrograms of these reconstructed signal estimates are shown in Fig. 14, where the gray scale is in units of source pressure spectral density (dB *re* μPa^2/Hz @ 1 m). The theoretical depth resolution of the MFP results presented here is expected to be within ± 2 m, because frequencies greater than 110 Hz were used in the inversions.

These narrow-band high-intensity regions (indicated by white arrows) are not propagation effects, but seem to be generated within the animal itself. Whenever a harmonic of the FM fundamental passes through this region, the signal level increases by around 5–10 dB.

III. DISCUSSION AND SPECULATIONS

A. General comments

The four whales tracked in this paper provide interesting insights into their acoustic behavior. While blue whales are capable of descending to 100-m depth to feed,[38] all the

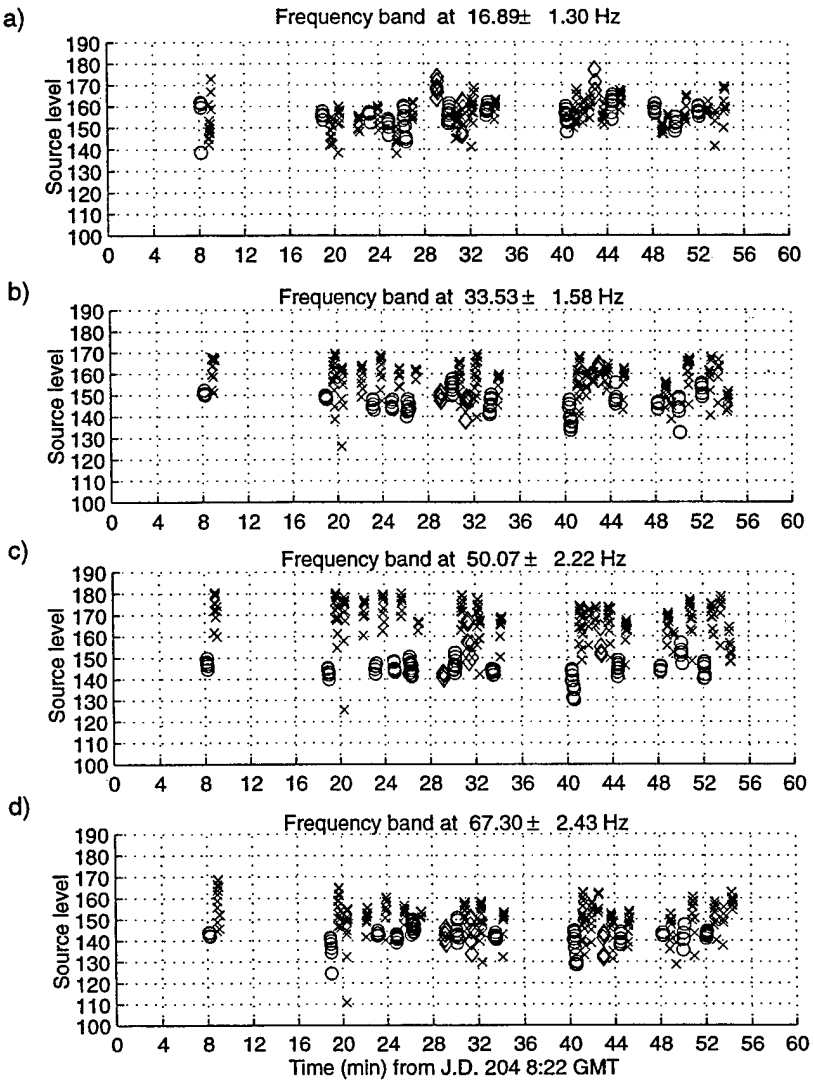

FIG. 13. Estimated source pressure spectral densities in different frequency bands of type A and B calls (dB *re* 1 μPa^2/Hz @ 1 m) for case 3. Call locations were estimated using 30-, 50-, and 65-Hz band information. Circles represent type A calls, "×" represents type B, and diamonds represent strongly modulated B and D calls. (a) 17-Hz band; (b) 33-Hz band; (c) 50-Hz band; (d) 67-Hz band.

whales tracked here vocalized between 10- and 40-m depth, whether stationary or transiting. The animal in case 3 yielded four complete dive profiles that show the animal's depth changes only gradually while calling. Most animals swam from east to west at rates of around 2–3 m/s, but one animal remained within 500 m of its original position for 45 min. The case 2 sequence tracked two vocalizing whales simultaneously, including a period when the animals passed within 2 km of each other. However, neither animal appeared to alter its course in response to the other's presence.

Having constructed an environmental propagation model, it is a simple matter to compute both the optimal frequency of propagation, and the depth at which an acoustic source should be placed to minimize transmission losses.[63] The optimum depth for transmitting frequencies between 10–150 Hz in a 130-m deep environment is about 80 m. Over a 10-km propagation range, a 17-Hz source shallower than 40 m would suffer a large transmission loss due to destructive interference between the source and surface reflection. Given the fact that most of the energy in blue whale vocalizations lie under 20 Hz, it seems clear that the vocalization depths of the animals were not acoustically optimized for propagation under the shallow-water conditions present around FLIP.

B. Do blue whales display an internal resonance?

The results of Sec. II D suggest the presence of a possible internal resonance within the animal. A mechanical resonance might be present in the oscillating source (generally assumed to be or near the arytenoid cartilages, see references in Ref. 64), or an air-filled space may act as a resonator that couples with the oscillator, similar in manner to the way the vibration of the double reed within an oboe is influenced by the resonant characteristics of the tube.[65]

The limited samples present here suggest an air-filled resonator may be more likely, because the frequency of this hypothetical resonance seems to increase with the animal's depth, which is what would be expected if an air-filled cavity were being compressed. Unfortunately, the depth-frequency relationship visible does not fit any simple resonator model. For example, the resonant frequency of a bubble of fixed size is proportional to the square root of the external pressure.[66] The first and last call depths are 20 and 30 m, so the resulting external water pressure increase is about 33%, and the expected frequency shift for a resonating bubble is 15%. The regions indicated by the arrows show a much greater frequency shift. In fact, the hypothetical resonance frequency seems to be proportional to the external pressure squared,

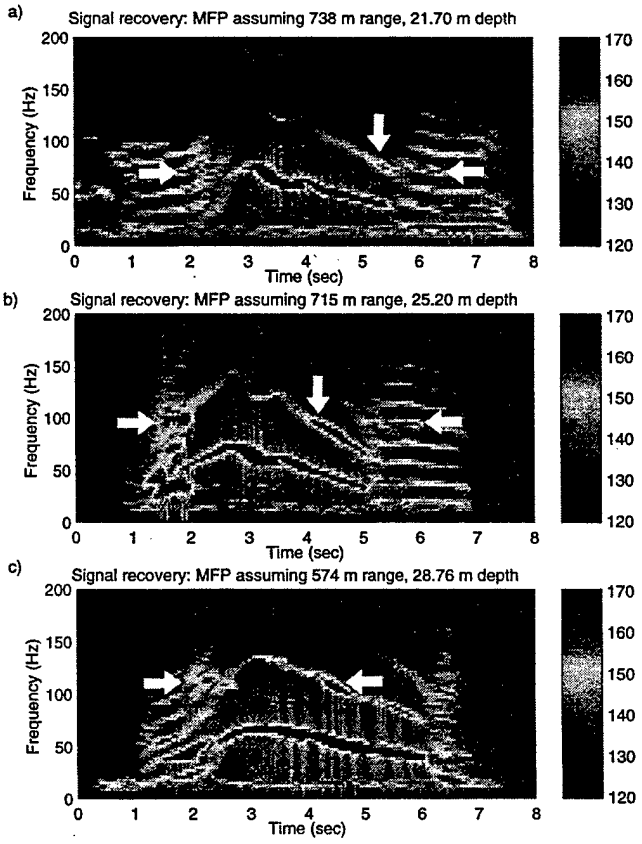

FIG. 14. Source pressure spectral density spectrograms (*re* dB *re* 1 μPa^2/Hz @ 1 m) of estimated source signatures for three "type D" FM downsweeps, obtained using multichannel deconvolution and an optimized inverted environment. White arrows indicate speculated resonances of sound-production mechanism: (a) Starting at J.D. 204, 8:51:18 GMT, 738±10 m range, 22 ±2 m depth. (b) Starting at J.D. 204, 8:51:45 GMT, 715±10 m range, 25 ±2 m depth. (c) Starting at J.D. 204, 8:53:28 GMT, 574±10 m range, 29 ±2 m depth.

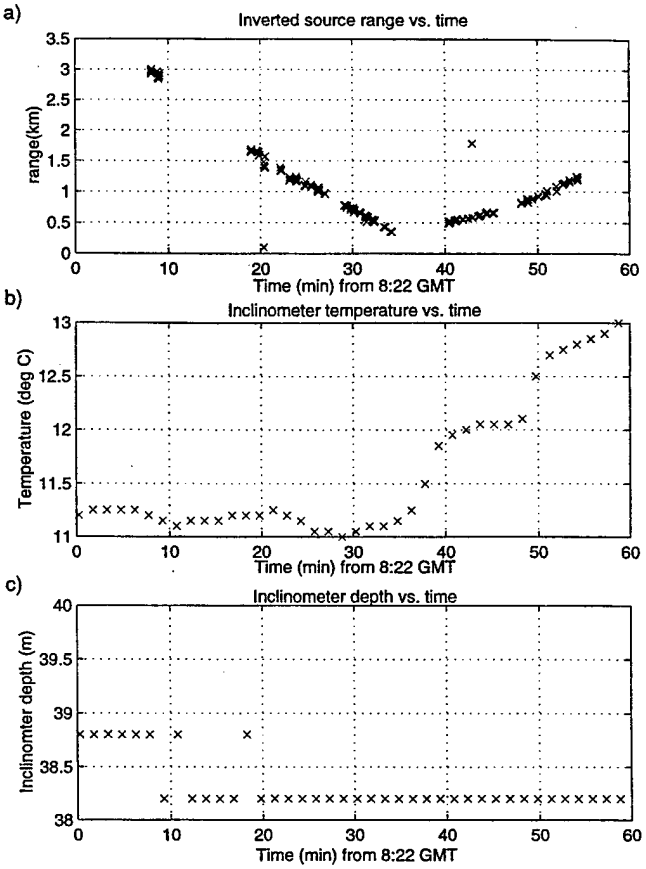

FIG. 15. Comparison between case 3 whale location and local environmental conditions. (a) Range track of blue whale versus time; (b) water temperature (°C) measured at inclinometer versus time; (c) measured inclinometer depth versus time.

instead of the square root. A Helmholtz resonator[66] would also show the same square root dependence on ambient pressure, and a bubble resonator allowed to collapse in volume with depth would still only show a linear dependence on external pressure. It is clear that more samples of these FM downsweeps would be required to answer these questions.

C. Do whales associate with tidal bores?

Another interesting feature associated with case 3 is that the animal's arrival corresponds with a sudden change in oceanic conditions. Figure 15 demonstrates this association by replotting the whale's range versus time in (a), the water temperature at the array inclinometer vs time in (b), and the inclinometer depth in (c). This last plot shows that the temperature change is not caused by a sudden change in the temperature sensor depth (note that the inclinometer depth measurements are quantized in increments of about 0.5 m).

To within the timing resolution of the inclinometer (90 s), the point at which the whale reached its closest approach to FLIP was associated with a 1.0 °C jump in water temperature, followed 10 min later by another 1.0 °C jump. The eventual total temperature increase is 2.5 °C over 30 min. During the previous 11 hours the temperature had remained within 0.5 of 11 °C. This temperature jump was the largest short-term temperature change recorded over the 42 hours of the experiment, and was accompanied by a rapid rotation in the array tilt direction from 300° bearing to about 200°. Unfortunately, heavy cloud cover in the area blocked any useful SST satellite measurements recorded at this time.

An examination of the complete temperature/array tilt record showed that three strong disturbances occur approximately every 12 hours, during which the water temperature rises quickly, and the array tilts to the south. The closest approach of the transiting whale in case 2 also took place in the middle of the previous strong disturbance. These disturbances last less than 2 hours, and then the ocean returns to baseline conditions. The 12-hour spacing of these events suggests a tidal mechanism, during times when the tide level is changing most rapidly. Such behavior might be associated with tidal bores generated along the shelf of San Miguel.[66]

There is anecdotal evidence[67] relating the sightings of whales and other sea life with the presence of strong ocean fronts. Recent work has shown that shorward-propagating internal bores concentrate zooplankton,[68] a propperty that might be exploited by a whale. However, more observations will be required to establish whether whales feed along tidal bores.

IV. CONCLUSION

Matched-field processing (MFP) and global inversion methods have been used to plot the three-dimensional trajec-

tories of four blue whales over periods of up to 90 min and ranges to 8 km. The information needed for the computational models was extracted from the whale calls themselves, using as few as eight hydrophones, spread over a 90-m depth. The extracted values for surface sediment sound-speed estimates lie within ± 50 m/s of those derived from sediment samples collected in the area. These results are believed to be the first successful three-dimensional localizations of a vocalizing baleen whale over long periods of time, and the first successful three-dimensional localizations of marine mammal vocalizations recorded at ranges greater than several water depths from the hydrophone.

The MFP localization and source signature recoveries have raised several interesting questions about the purpose and production mechanism for these calls. The whale in case 3 produced heavily modulated signals that were not stereotyped, atypical behavior for blue whales in this region. In addition, the source level of its fundamental frequency was nearly 20 dB lower than the whales in case 2. These two feature suggest the possibility that this animal might have been a juvenile. This whale's arrival also closely coincided with the arrival of a prominent but short-lived ocean disturbance that changed the ocean temperature by over 2.0 °C over 20 min. Finally, certain FM downsweeps made by this animal display signs of an internal resonance that may be depth-dependent.

Clearly much remains to be learned about the natural acoustic lives of baleen whales, as well as their responses to short- and long-term anthropogenic activities. We hope the potential of some powerful new tools to address these questions has been demonstrated.

ACKNOWLEDGMENTS

The authors would like to thank MPL technical staff and the crew of the R/P FLIP for making the collection of the data used in this paper possible. In particular, the assistance of James Murray and Dave Ensberg is particularly appreciated. They would also like to thank myriad individuals within the Southwest Fisheries Science Center, including Paul Fielder, Alexandra von Saunder, Wayne Perryman, and Jay Barlow. Stu Smith of the Geological Data Center at Scripps provided us with bathymetric information, and useful sediment data was provided by Donn Gorsline of the Department of Marine Geology of the University of Southern California. Peter Gerstoft wrote the extremely useful genetic algorithm inversion package SAGA, and provided a great deal of advice on how to use it. Lisa Schlender of Cascadia Research tried to identify the individual whales videotaped on Julian Day 203. Mike Porter, Mark McDonald, and Dave Mellinger contributed helpful suggestions and insights to the paper. Demultiplexing of the DIFAR sonobuoy data was conducted using software acquired from Greeneridge Sciences, Inc., in Santa Barbara, California. This research was funded by the Office of Naval Research Grant Nos. N00014-97-0593 and N00014-96-1-0603.

[1] A. B. Baggeroer, W. A. Kuperman, and P. N. Mikhalevsky, "An overview of matched field methods in ocean acoustics," IEEE J. Ocean Eng. **18**, 401–424 (1993).

[2] F. B. Jensen, W. A. Kuperman, M. B. Porter, and H. Schmidt, *Computational Ocean Acoustics* (AIP, New York, 1994).

[3] A. B. Baggeroer, W. A. Kuperman, and H. Schmidt, "Matched field processing: Source localization in correlated noise as an optimum parameter estimation problem," J. Acoust. Soc. Am. **83**, 571–587 (1988).

[4] G. D'Spain, W. A. Kuperman, W. S. Hodgkiss, and L. P. Berger, "3-D localization of a blue whale," Scripps Institution of Oceanography, Technical Memorandum MPL TM 447 (1995).

[5] G. L. D'Spain, W. A. Kuperman, W. S. Hodgkiss, and L. P. Berger, "Three-dimensional localization of a blue whale using broadband matched-field processing for range and depth, and plane-wave adaptive beamforming for azimuth," J. Acoust. Soc. Am. **97**, 3353 (A) (1995).

[6] G. L. D'Spain, W. A. Kuperman, C. W. Clark, and D. K. Mellinger, "Simultaneous source ranging and bottom geoacoustic inversion using shallow water, broadband dispersion of fin whale calls," J. Acoust. Soc. Am. **97**, 3353 (A) (1995).

[7] "Sonobuoy Instruction Manual," Naval Weapons Support Center NAVAIR 28-SSQ-500-1 (1983).

[8] K. M. Stafford, C. G. Fox, and D. S. Clark, "Long-range acoustic detection and localization of blue whale calls in the northeast Pacific Ocean," J. Acoust. Soc. Am. **104**, 3616–3625 (1998).

[9] M. A. McDonald, J. A. Hildebrand, and S. C. Webb, "Blue and fin whales observed on a seafloor array in the Northeast Pacific," J. Acoust. Soc. Am. **98**, 712–21 (1995).

[10] A. M. Teranishi, J. A. Hildebrand, M. A. McDonald, S. E. Moore, and K. M. Stafford, "Acoustic and visual studies of blue whales near the California Channel Islands," J. Acoust. Soc. Am. **102**, 3121 (1997).

[11] M. A. McDonald and C. G. Fox, "Passive acoustic methods applied to fin whale population density estimation," J. Acoust. Soc. Am. **1015**, 2643–2651 (1999).

[12] W. A. Watkins and W. E. Schevill, "Sound source location by arrival times on a non-rigid three-dimensional hydrophone array," Deep-Sea Res. **19**, 691–706 (1972).

[13] L. E. Freitag and P. L. Tyack, "Passive acoustic localization of the Atlantic bottlenose dolphin using whistles and echolocation clicks," J. Acoust. Soc. Am. **93**, 2197–2205 (1993).

[14] D. E. McGehee, "1997 Sperm Whale Abundance and Population Structure Cruise Leg II Sonobuoy Project, Final Report," Tracor Applied Sciences T-97-56-0002-U (1997).

[15] S. Finette, P. C. Mignerey, and J. F. Smith, "Broadband source signature extraction using a vertical array," J. Acoust. Soc. Am. **94**, 309–318 (1993).

[16] P. C. Mignerey and S. Finette, "Multichannel deconvolution of an acoustic transient in an oceanic waveguide," J. Acoust. Soc. Am. **92**, 351–364 (1992).

[17] J. A. Rivers, "Blue whale, *Balaenoptera musculus*, vocalizations from the waters off central California," Marine Mammal Science **13**, 186–195 (1997).

[18] P. O. Thompson, L. T. Findley, O. Vidal, and W. C. Cummings, "Underwater sounds of blue whales, *Balaenoptera musculus*, in the Gulf of California, Mexico," Marine Mammal Science **12**, 228–293 (1996).

[19] A. Alling, E. M. Dorsey, and J. C. D. Gordon, "Blue whales (*Balaenoptera musculus*) off the Northeast Coast of Sri Lanka: Distribution, feeding and individual identification," in *Cetaceans and Cetacean Research in the Indian Ocean Sanctuary*, United Nations Mar. Mammal. Tech. Rep. 3, edited by S. Leatherwood and G. P. Donovan (Nairobi, Kenya, 1991), pp. 248–258.

[20] W. C. Cummings and P. O. Thompson, "Underwater sounds from the blue whale, *Balaenoptera musculus*," J. Acoust. Soc. Am. **50**, 1193–1198 (1971).

[21] P. L. Edds, "Vocalizations of the blue whale, *Balaenoptera musculus*, in the St. Lawrence River," J. Mammal. **63**, 345–347 (1982).

[22] A. C. Kibblewhite, R. N. Denham, and D. J. Barnes, "Unusual low-frequency signals observed in New Zealand waters," J. Acoust. Soc. Am. **41**, 644–655 (1967).

[23] D. K. Mellinger and C. W. Clark, "Characteristics of fin and blue whale vocalizations recorded from IUSS in the north and west Atlantic," 11th Biennial Conference on the Biology of Marine Mammals, Orlando, FL, 1995.

[24] J. W. Northrup and W. C. Cummings, "Underwater 20-Hz signals recorded near Midway Island," J. Acoust. Soc. Am. **49**, 1909–1910 (1971).

[25] P. O. Thompson and W. A. Friedl, "A long term study of low frequency sounds from several species of whales off Oahu, Hawaii," Cetology **19**, 1–19 (1982).

[26] J. S. Perkins and W. A. Kuperman, "Environmental signal processing: Three-dimensional matched-field processing with a vertical array," J. Acoust. Soc. Am. **87**, 1553–1556 (1990).
[27] N. O. Booth, P. A. Baxley, J. A. Rice, P. W. Schey, W. S. Hodgkiss, G. L. D'Spain, and J. J. Murray, "Source localization with broad-band matched-field processing in shallow water," IEEE J. Ocean Eng. **21**, 402–412 (1996).
[28] M. D. Collins and W. A. Kuperman, "Focalization: Environmental focusing and source localization," J. Acoust. Soc. Am. **90**, 1410–1422 (1991).
[29] D. F. Gingras and P. Gerstoft, "Inversion for geometric and geoacoustic parameters in shallow water: Experimental results," J. Acoust. Soc. Am. **97**, 3589–3598 (1995).
[30] S. E. Dosso, M. L. Yeremy, J. M. Ozard, and N. R. Chapman, "Estimation of ocean bottom properties by matched-field inversion of acoustic field data," IEEE J. Ocean Eng. **18**, 232–239 (1993).
[31] P. Gerstoft, "Inversion of seismoacoustic data using genetic algorithms and a posteriori probability distributions," J. Acoust. Soc. Am. **95**, 770–782 (1994).
[32] P. Gerstoft, "Inversion of acoustic data using a combination of genetic algorithms and the Gauss-Newton approach," J. Acoust. Soc. Am. **97**, 2181–2190 (1995).
[33] P. Gerstoft and D. F. Gingras, "Parameter estimation using multifrequency range-dependent acoustic data in shallow water," J. Acoust. Soc. Am. **99**, 2839–2851 (1996).
[34] P. Gerstoft, "SAGA Users Guide 2.0, an inversion software package," SACLANT Undersea Research Centre SM-333 (1997).
[35] E. D. Bronson and L. R. Glosten, "FLIP; Floating Instrument Platform," Marine Physical Laboratory, SIO, MPL Tech. Memo MPL-U-27/85 (1985).
[36] "http://www.nos.noaa.gov/ocrm/nmsp/nmschannelislands.html," Vol. 1996, NOAA, 1999.
[37] K. F. Mangels and P. Fiedler, "Cruise announcement: Whale habitat and prey study (WHAPS95), a marine mammal habitat survey off southern California," U. S. Dept. of Commerce, Nat'l Oceanic and Atmos. Admin., Nat'l Marine Fish. Service, Southwest Fish. Sci. Center, Feb (1995).
[38] P. C. Fiedler, S. Reilly, R. P. Hewitt, D. Demer, V. A. Philbrick, S. Smith, W. Armstrong, D. A. Croll, B. R. Tershey, and B. R. Mate, "Blue whale habitat and prey in the Channel Islands," Deep-Sea Res. II **45**, 1781–1801 (1998).
[39] W. S. Hodgkiss, J. C. Nickles, G. L. Edmonds, R. A. Harriss, and G. L. D'Spain, "A large dynamic range vertical array of acoustic sensors," *Full Field Inversion Methods in Ocean and Seismic Acoustics,* edited by O. Diachok (Kluwer, Dordrecht, The Netherlands, 1995).
[40] G. L. D'Spain and W. S. Hodgkiss, "Array processing with acoustic measurements at a single point in the ocean," J. Acoust. Soc. Am. **91**, 2364 (A) (1992).
[41] G. L. D'Spain, W. S. Hodgkiss, and G. L. Edmonds, "Energetics of the deep ocean's infrasonic sound field," J. Acoust. Soc. Am. **89**, 1134–1158 (1991).
[42] L. Davis, *Genetic Algorithms and Simulated Annealing* (Pitman, London, 1987).
[43] D. E. Goldberg, *Genetic Algorithms in Search, Optimization, and Machine Learning* (Addison-Wesley, Reading, MA, 1989).
[44] M. B. Porter, "The KRAKEN normal mode program," SACLANTCEN, Memorandum SM-245, 1991.
[45] J.-M. Q. D. Tran and W. S. Hodgkiss, "Sound-speed profile inversion using a large aperture vertical line array," J. Acoust. Soc. Am. **93**, 803–812 (1993).
[46] P. O. Thompson, "20-Hz pulses and other vocalizations of fin whales, *Balaenoptera physalus*, in the Gulf of California, Mexico," J. Acoust. Soc. Am. **92**, 3051–3057 (1992).
[47] W. A. Watkins, "Activities and underwater sounds of fin whales," Sci. Rep. Whal. Res. Inst. **33**, 83–117 (1981).
[48] W. A. Watkins, P. Tyack, K. E. Moore, and J. E. Bird, "The 20-Hz signals of finback whales (*Balaenoptera physalus*)," J. Acoust. Soc. Am. **82**, 1901–1912 (1987).
[49] W. J. Richardson, C. R. Greene, C. I. Malme, and D. H. Thomson, *Marine Mammals and Noise* (Academic, San Diego, 1995).
[50] J. Northrop, W. Cummings, and P. Thompson, "20-Hz signals observed in the central Pacific," J. Acoust. Soc. Am. **43**, 383–384 (1968).
[51] H. Cox, R. M. Zeskind, and M. M. Owen, "Robust adaptive beamforming," IEEE Trans. Acoust., Speech, Signal Process. **35**, 1365–1375 (1987).
[52] R. A. Gramann, "ABF algorithms implemented at ARL:UT," Applied Research Laboratories, University of Texas, ARL-TL-EV-92-31 (1992).
[53] P. K. Yochem and S. Leatherwood, "Blue Whale," in *Handbook of Marine Mammals,* edited by S. H. Ridgway and S. R. Harrison (Harcourt Brace Jovanovich, San Diego, 1985), Vol. 3, p. 223.
[54] G. L. D'Spain, J. J. Murray, W. S. Hodgkiss, N. O. Booth, and P. W. Schey, "Mirages in shallow water matched field processing," J. Acoust. Soc. Am. **105**, 3245–3265 (1999).
[55] W. Perryman, personal communication, 1996.
[56] M. D. Collins, R. J. Cederberg, D. B. King, and S. A. Chin-Bing, "Comparison of algorithms for solving parabolic wave equations," J. Acoust. Soc. Am. **100**, 178–82 (1996).
[57] W. A. Kuperman, M. B. Porter, and J. S. Perkins, "Rapid computation of acoustic fields in three-dimensional ocean environments," J. Acoust. Soc. Am. **89**, 125–33 (1991).
[58] E. L. Hamilton, "Geoacoustic modeling of the sea floor," J. Acoust. Soc. Am. **68**, 1313–1339 (1980).
[59] D. Gorsline, unpublished station data, 1997.
[60] R. T. Bachman, "Estimating velocity ratio in marine sediment," J. Acoust. Soc. Am. **86**, 2029–2031 (1989).
[61] T. C. Yang, "Broadband source localization and signature estimation," J. Acoust. Soc. Am. **93**, 1797–1806 (1993).
[62] S. D. Chuprov, "Interference structure of a sound field in a layered ocean," in *Akustika Okeana. Sovremennoe sostoyanie* (*Ocean Acoustics, Current State*), edited by L. M. Brekhovskikh and I. B. Andreevoi (Nauka, Moscow, 1982), pp. 71–91.
[63] F. B. Jensen and W. A. Kuperman, "Optimum frequency of propagation in shallow water environments," J. Acoust. Soc. Am. **73**, 813–819 (1983).
[64] M. A. McDonald, J. A. Hildebrand, and S. C. Webb, "On the sound production mechanism of blue whales" (unpublished).
[65] N. H. Fletcher, *The Physical of Musical Instruments* (Springer-Verlag, New York, 1991).
[66] M. Hendershott, personal communication, 1999.
[67] J. Barlow, personal communication, 1999.
[68] J. Pineada, "Circulation and larval distribution in internal tidal bore warm fronts," Limnology and Oceanography **44**, 1400–1414 (1999).